Phenomenological Ginzburg-Landau-like theory for superconductivity in the cuprates

Sumilan Banerjee*, T. V. Ramakrishnan*+, and Chandan Dasgupta*

* Centre for Condensed Matter Theory, Department of Physics,
Indian Institute of Science, Bangalore 560012, India
+ Department of Physics, Banaras Hindu University, Varanasi 221005, India

We propose and develop here a phenomenological Ginzburg-Landau-like theory of cuprate high-temperature superconductivity. The free energy of a cuprate superconductor is expressed as a functional $\mathcal{F}$ of the complex spin-singlet pair amplitude $\psi_{ij} \equiv \psi_m = \Delta_m \exp(i\phi_m)$ where i and j are nearest-neighbor sites of the square planar Cu lattice in which the superconductivity is believed to primarily reside and m labels the site located at the center of the bond between i and j. The system is modeled as a weakly coupled stack of such planes. We hypothesize a simple form, $\mathcal{F}[\Delta, \phi] = \sum_m (A\Delta_m^2 + (B/2)\Delta_m^4) + C \sum_{<mn>} \Delta_m \Delta_n \cos(\phi_m - \phi_n)$, for the functional, where m and n are nearest-neighbor sites on the bond-center lattice. This form is analogous to the original continuum Ginzburg-Landau free energy functional; the coefficients A, B and C are determined from comparison with experiments. A combination of analytic approximations, numerical minimization and Monte Carlo simulations is used to work out a number of consequences of the proposed functional for specific choices of A, B and C as functions of hole density x and temperature T. There can be a rapid crossover of $\langle \Delta_m \rangle$ from small to large values as A changes sign from positive to negative on lowering T; this crossover temperatures $T_{\mathrm{ms}}(x)$ is identified with the observed pseudogap temperature $T^*(x)$. The thermodynamic superconducting phase-coherence transition occurs at a lower temperature $T_c(x)$, and describes superconductivity with d-wave symmetry for positive C. The calculated $T_c(x)$ curve has the observed parabolic shape. The results for the superfluid density $\rho_s(x,T)$, the local gap magnitude $\langle \Delta_m \rangle$, the specific heat $C_v(x,T)$ (with and without a magnetic field) as well as vortex properties, all obtained using the proposed functional, are compared successfully with experiments. We also obtain the electron spectral density as influenced by the coupling between the electrons and the correlation function of the pair amplitude calculated from the functional and compare the results successfully with the electronic spectrum measured through Angle Resolved Photoemission Spectroscopy (ARPES). For the specific heat, vortex structure and electron spectral density, only some of the final results are reported here; the details are presented in subsequent papers.

I. INTRODUCTION

The last two decades have seen unprecedented experimental and theoretical activities involving cuprates which exhibit high-temperature superconductivity [1–4]. Even after this long period of research which has seen dramatic advances in experimental techniques and materials quality, as well as discovery of many unusual phenomena such as the ubiquitous pseudogap in underdoped cuprates [5–8] and the 'strange metal' phase above the superconducting transition temperature around optimal doping [1–3], there is no common, broadly accepted understanding yet about their origin.

Motivated by the above, especially the increasing volume of sophisticated spectroscopic data on the cuprates (such as those obtained from ARPES [9, 10], STM [11] and Raman [12] experiments), we propose and develop here, as well as in subsequent papers, a new phenomenological model for cuprate superconductivity that is analogous in form to the well-known Ginzburg-Landau (GL) theory [13] of superconductivity. The starting point of our description is the assumption that the free energy of a cuprate superconductor can be expressed as a functional solely of the complex pair amplitude. In the original continuum GL theory, the free energy, expressed as a functional of the complex order parameter field

$\psi(\mathbf{r}) = \Delta(\mathbf{r}) \exp(i\phi(\mathbf{r}))$, has the form

$$
\begin{aligned}
\mathcal{F}(\{\psi(\mathbf{r})\}) &= \int d\mathbf{r} \left[A_c |\psi(\mathbf{r})|^2 + \frac{B_c}{2} |\psi(\mathbf{r})|^4 \right. \\
&\quad \left. + \frac{C_c}{2} |\boldsymbol{\nabla}\psi(\mathbf{r})|^2 \right].
\end{aligned}
\tag{1}
$$

This form is justified near the actual superconducting transition where the magnitude of the order parameter is small, so that a low-order power series expansion in $\psi(\mathbf{r})$ is adequate. Further, $\psi(\mathbf{r})$ is assumed to vary slowly with $\mathbf{r}$ so that it suffices to keep only the $|\boldsymbol{\nabla}\psi(\mathbf{r})|^2$ term; this is the case in conventional superconductors where the natural superconducting length scale (also the coarse graining scale) ξ_0 is large (compared, say, to the Fermi wavelength). After the advent of the microscopic Bardeen-Cooper-Schrieffer (BCS) [14] theory of superconductivity, $\psi(\mathbf{r})$ was identified by Gor'kov [15] with the Cooper pair amplitude, i.e. $\psi(\mathbf{r}) = \langle a_\uparrow(\mathbf{r}) a_\downarrow(\mathbf{r}) \rangle$, where $a_\sigma(\mathbf{r})$ ($a_\sigma^\dagger(\mathbf{r})$) is the operator which destroys (creates) an electron at $\mathbf{r}$ with spin σ ($\sigma =\uparrow, \downarrow$). Gor'kov also obtained the coefficients A_c, B_c, C_c in terms of the electronic parameters of the metal.

In our phenomenological description, we hypothesize that a free energy functional similar in structure to that of Eq.(1), but defined on the square planar CuO$_2$ lattice, describes the properties of cuprate superconductors for a
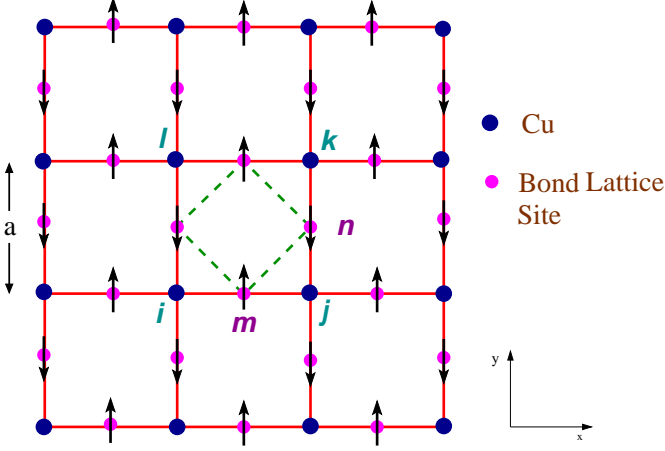
FIG. 1: The square Cu lattice sites $i, j, k, l, ..$ in the CuO_2 plane and construction of the bond lattice out of the centers of the Cu-O-Cu bonds. The solid circles at $\{\mathbf{R}_i \doteq i\}$ (blue) represent the positions of Cu lattice sites and $\{\mathbf{R}_m \doteq m \equiv ij\}$ (magenta) the positions of bond centre lattice sites. Alternatively, we denote the bond centre lattice site between $\mathbf{R}_i$ and $\mathbf{R}_j = \mathbf{R}_i + a\hat{\mu}$ as $\mathbf{R}_{i\mu} \equiv \mathbf{R}_i + (a/2)\hat{\mu}$ with $\hat{\mu} = +\hat{x}, +\hat{y}$. The arrows indicate the direction of equivalent planar spins, with $\mathbf{S}_m = (\Delta_m \cos\phi_m, \Delta_m \sin\phi_m)$ representing the complex order parameter $\psi_{ij} \equiv \psi_m = \Delta_m \exp(i\phi_m)$ and antiferromagnetic ordering (shown) of spins translating into a d-wave symmetry gap (long-range order).

FIG. 2: A schematic illustration of the hole doping x and temperature T plane (entire shaded region) where we assume the functional of Eq.(2) to be applicable. $T_l^0(x)$ (solid brown line) and $T_c(x)$ (solid blue line) are shown along with the experimental superconducting (SC) dome and antiferromagnetic (AF) regime at very low hole doping. The two arcs shown by dotted lines denote regions where quantum fluctuation effects, as well as other low-energy degrees of freedom, such as electronic and spin plus their coupling with pair degrees of freedom, need to be explicitly included in the free energy functional. For instance, inclusion of quantum phase fluctuation effects in a minimal level leads to a $T_c(x)$ curve in agreement with experiment (See Section III).

fairly wide range of hole doping (x) and temperature (T). Fig.1 shows the square planar lattice schematically, and Fig.2 the region of the (x, T) plane where our phenomenological description is assumed to be applicable. The free energy is assumed to be a functional of the complex spin-singlet pair amplitude $\psi_{ij} \equiv \psi_m = \Delta_m \exp(i\phi_m)$ where i and j are nearest-neighbor sites of the square planar Cu lattice and m labels the 'bond-center lattice' site located at the center of the bond between the lattice sites i and j (see Fig. 1). The highly anisotropic cuprate superconductor is modeled as a weakly coupled stack of CuO_2 planes in which the superconductivity is believed to primarily reside and we ignore, as a first approximation, the interplane coupling. The free energy functional for a single CuO_2 plane is assumed to have the form

$$\mathcal{F}(\{\Delta_m, \phi_m\}) = \mathcal{F}_0(\{\Delta_m\}) + \mathcal{F}_1(\{\Delta_m, \phi_m\}), \quad (2a)$$

$$\mathcal{F}_0(\{\Delta_m\}) = \sum_m \left(A\Delta_m^2 + \frac{B}{2}\Delta_m^4 \right), \quad (2b)$$

$$\mathcal{F}_1(\{\Delta_m, \phi_m\}) = C \sum_{<mn>} \Delta_m \Delta_n \cos(\phi_m - \phi_n) \quad (2c)$$

A Gor'kov like interpretation of ψ_{ij} is that it is the average spin-singlet nearest-neighbor Cooper pair amplitude, i.e. $\psi_{ij} = \langle b_{ij} \rangle / \sqrt{2} = (1/2)\langle a_{i\downarrow}a_{j\uparrow} - a_{i\uparrow}a_{j\downarrow} \rangle$. The sites i and j are different because strong electron repulsion (symbolized for example by the Mott-Hubbard U) disfavors on-site pairing, while the existence of large nearest-
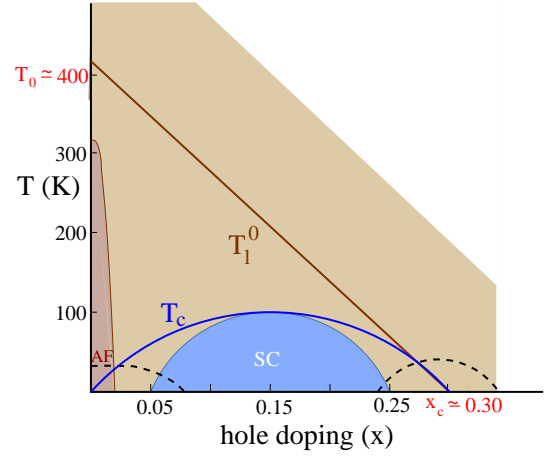
neighbor antiferromagnetic spin-spin interaction in the parent cuprate is identically equivalent for spin-$\frac{1}{2}$ electrons to attraction between nearest-neighbor pairs (i.e. $J_{ij}(\mathbf{S}_i.\mathbf{S}_j - \frac{1}{4}\hat{n}_i\hat{n}_j) = -J_{ij}b_{ij}^\dagger b_{ij}$ with $\mathbf{S}_i$ and $\hat{n}_i$ the electron spin and number operators respectively at the i-th site). This favors the formation of nearest-neighbor spin-singlet pairs.

The first part $\mathcal{F}_0$ of $\mathcal{F}$ is the sum of identical independent terms each of which is a function of only the magnitude Δ_m of the order parameter on the bond lattice site. Eq.(2b) is a simple form for it in the image of Eq.(1), with A and B depending, in general, on x and T. We assume that B is a positive constant independent of x and T and choose $A(x, T)$ to change sign along a straight line $T_l^0(x)$ running from $T = T_0$ at $x = 0$ to $T = 0$ at $x = x_c$ (see Fig. 2). As a first approximation, this line can be identified with the pseudogap temperature $T^*(x)$ because the magnitude of the local pair ampliitude, $\langle \Delta_m \rangle$, can increase dramatically as the temperature crosses this line, so that A changes from a positive to a negative value. The occurrence of superconductivity, characterized by a nonzero stiffness for long-wavelength phase fluctuations and the associated superconducting phase coherence, depends on the phase coupling term, Eq.(2c). If C in Eq.(2c) is taken to be proportional to x, the superconducting transition temperature T_c, as calculated in our theory, turns out to be proportional to x for

small values of it, in conformity with what is observed, e.g. the Uemura correlation [16]. Also, if C is taken to be positive, the transition is to a d-wave symmetry superconducting state (see Section II). We, therefore, make this choice.

We emphasize that the assumed form of the functional and the dependence of the coefficients on x and T are purely phenomenological, guided by experimental results – the functional is not derived from a microscopic theory. The functional satisfies the usual symmetry and stability requirements: the absence of odd powers of ψ_m ensures invariance of the free energy under a global change of phase, and the free energy is bounded below for the chosen positive B. Since $\Delta_m = |\psi_m|$ and $\Delta_m \Delta_n \cos(\phi_m - \phi_n) = -(|\psi_m - \psi_n|^2 - \Delta_m^2 - \Delta_n^2)/2$, it is readily seen that the free energy of Eq.(2) is similar in form to a discretized version of the GL functional of Eq.(1). However, there are important differences between our phenomenological approach and the original GL theory – these differences are discussed in detail in Section II.

The main objective of our study is to investigate whether the free energy functional defined above provides a good description of experimental results over a wide range of x and T. To this end, we have carried out several investigations of the thermodynamic behavior of a system whose equilibrium properties are given by canonical (thermal) averages with the functional of Eq.(2) playing the role of the 'Hamiltonian' or energy function. These calculations have been performed at several levels of sophistication. We first used simple single-site mean-field theory to obtain qualitative information about the behavior of the system over a wide range of x and T. We also used cluster mean-field theory to obtain more accurate estimates of the superconducting transition temperature as a function of doping. We used numerical minimization of the free energy to obtain exact results for the properties of the system and the structure of vortices at zero temperature. We also used extensive Monte Carlo (MC) simulations to obtain exact (modulo finite-size effects) information about the thermodynamic behavior of the system at finite temperatures. Since the free energy of Eq.(2) may be viewed as the Hamiltonian of a two-dimensional XY model with fluctuations in the magnitudes of the 'spins' (see Section II for the details of this analogy), we made use of well-known results about the behavior of the XY model in two dimensions in the analysis of the data obtained from our MC simulations. Finally, we extended our free energy functional to include quantum phase fluctuations (see Section III) in order to study the effects of these fluctuations on the transition temperature, and included coupling of the pair degrees of freedom to electrons (see Section VIII) to study the spectral properties of electrons measured in ARPES experiments. Simple, physically motivated, approximate analytic methods were used in these studies. The main results obtained from these extensive analytic and numerical calculations are summarized below.

As a starting point, we calculate the superconducting transition temperature $T_c(x)$ and the average magnitude of the local pair amplitude, $\langle \Delta_m \rangle$, using single-site mean-field theory for the model of Eq.(2). We show that this approximation leads to general features of the $x-T$ phase diagram in agreement with experiment. In particular, we find a phase coherent superconducting state with d-wave symmetry below a parabolic $T_c(x)$ dome and a phase incoherent state with a perceptible local gap that persists up to a temperature around $T_l^0(x)$. Further, effects of thermal fluctuations beyond the mean-field level are captured via MC simulations of the model of Eq.(2) for a finite two-dimensional lattice. Section III describes the results for $T_c(x)$ obtained from these simulations. The actual values of A, B and C used in these calculations are discussed in Section II.

The superfluid stiffness $\rho_s(x, T)$ (a quantity measured e.g. via the penetration depth) is calculated in Section IV. Its doping and temperature dependence compare well with experimental results [17–21]. The thermally averaged local gap $\bar{\Delta}(x, T) \equiv \langle \Delta_m \rangle$ is obtained in Section V where we calculate the temperature $T_{\rm ms}(x)$ corresponding to the maximum slope of this quantity with and without the C term. This temperature provides a measure of the pseudogap temperature $T^*(x)$. We use these results to remark on contrasting scenarios [7, 8] proposed for the doping dependence of the pseudogap. We find that there is a contribution to $\bar{\Delta}(x, T)$ that 'turns on' at $T_c(x)$, the superconducting transition temperature. This is obviously connected with persistent observations of two different kinds of energy gaps in several experiments [22, 23]. We also calculate the ratio $2\Delta(x, 0)/T_c(x)$ which is observed to be generally much larger than the BCS value of about 4 over a wide range of x [11, 24], and to vary from system to system within the cuprate family for the same x. Our results rationalize this behavior, which is expected here since the origins of $\Delta(x, 0)$ and T_c are different.

The contribution of the pair degrees of freedom to thermal properties, such as the specific heat C_v, can be obtained from the free energy functional of Eq.(2). We briefly report in Section VI our calculation of C_v (details are given in a subsequent paper [25]), and find that there are two peaks [26–29] in it, a sharp one connected with T_c (ordering of the phase of ψ_m) and a relatively broad one ('hump') linked to T^* (rapid growth of the magnitude of ψ_m). The former is specially sensitive to the presence of a magnetic field, as we find in agreement with experiment [30, 31]. Vortices, which are topological singularities in phase, are naturally explored in our approach [32]. We use the functional of Eq.(2) to find Δ_m and ϕ_m at different sites m for a 2π vortex whose core is at the center of a square plaquette of Cu lattice sites (Section VII). We find that the vortex changes character from being primarily a phase or Josephson vortex for small x to a more BCS-like vortex with a large diminution in the magnitude Δ_m as one approaches the vortex core for large x. Ref. [33] describes these results in greater detail.

Experimental information about the pair field ψ_m and its correlations is not obtained directly, but from its coupling to electrons (e.g. ARPES [9, 10] and STM [11]), photons (e.g. Raman scattering [12] and light absorption [34]) and neutrons [4]. We therefore develop a theory for the coupling of electrons near the Fermi energy with ψ_m and outline it in Section VIII. A separate paper [35] describes this approach in detail as well as the results (e.g. Fermi arcs that are ubiquitous above T_c, and the pseudogap for various momentum regions of the Fermi surface, especially the antinodal region) which compare very well with the results of recent ARPES measurements. We present here the results for the antinodal pseudogap filling temperature $T^{\rm an}(x)$ and compare it with the other estimate of the pseudogap temperature, $T_{\rm ms}(x)$, obtained in Section V.

The results summarized above establish that the simple free energy functional proposed here provides a consistent and qualitatively correct (quantitative in some cases) description of a variery of experimentally observed properties of cuprate superconductors over a wide range of temperature T and hole concentration x. This is the main conclusion of our study. Section IX discusses certain generalizations, applications and limitations of the approach used in our study. Appendices A, B and C describe some technical details of the calculations.

II.   THE FREE ENERGY FUNCTIONAL

A.   Generalities

As noted above, the free energy functional used in our study is phenomenological in nature with experimentally inspired coefficients. We have deliberately kept it as simple as possible, without violating basic requirements of symmetry and stability. The form of the functional of Eq.(2) is analogous to that used in conventional GL theory. However, our approach is different from the GL theory in several ways. The form of the free energy functional used in the GL theory of supercoductivity and in similar theories of other continuous phase transitions [36] can be justified only if the temperature is close to the transition temperature. This approach, therefore, is expected to yield quantitatively correct results only in the vicinity of the superconducting transition. This regime of validity is ordained by the requirement of smallness and slow spatial variation of the order parameter. Our use of the simple, GL-like functional of Eq.(2) over a broad (x, T) region can not be justified from similar considerations: the validity of our approach can only be judged a posteriori by comparing its consequences with experiments. Hence, we have calculated a variety of experimentally measurable quantities using the functional of Eq.(2) and compared the results with those of experiments. As discussed in detail in subsequent Sections, we find qualitative (and quantitative in some cases) agreement between the theoretical and experimental results for

a wide variety of properties of cuprate superconductors. This establishes the usefulness of our phenomenological approach in describing the properties of cuprate superconductors over a wide range of x and T.

Another important difference between our approach and conventional GL theory is that the free energy functional we consider is not coarse-grained in the GL sense. We believe that this is natural because all cuprate superconductors are characterized by short intrinsic pairing length scales or coarse-graining lengths ($\xi_0 \sim 15-20$ $\mathring{A}$ in the cuprates rather than the value of $\sim 10,000$ $\mathring{A}$ for 'conventional' pure superconductors). We thus use a 'nearest-neighbor' coupling of the pair amplitudes defined at the sites of the atomic bond lattice in the second term of our functional (Eq.(2c)). Another difference between the functional used in our study and that of conventional GL theory is that the sign of the coupling constant C in Eq.(2c) is taken to be *positive*, so that the pair amplitudes at nearest-neighbor sites of the bond-center lattice have a phase difference of π in the ground state. This difference in sign between the pair amplitudes on the 'horizontal' (in the x-direction) and 'vertical' (y-direction) bonds of the Cu lattice corresponds to the superconducting state having d-wave symmetry. This is consistent with the experimental fact that the superconducting gap $\Delta_{\mathbf{k}}$ is proportional to $(\cos k_x a - \cos k_y a)$, which arises in our description from a combination of nearest-neighbor Cooper pairs with relative phases as mentioned above.

Some of the methods of calculation used in our study are also different from that in the conventional GL theory of superconductivity in which physical properties are calculated using simple mean field theory. The mean-field results are expected to be valid if the temperature is outside the so-called 'critical' region [36] around the transition temperature where the effects of fluctuations, not included in a mean-field analysis, are important. For conventional superconductors with long coherence lengths, the width of the critical region is very small, so that mean field theory provides a good description of most of the experimentally observed behavior. This, however, is not the case for cuprate superconductors with very short coherence lengths and for our model of cuprate superconductivity. For this reason, we have to go beyond mean field theory (which provides a qualitatively correct, but not quantitative description of the general behavior) and use other methods (such as MC simulations) to obtain accurate results for the thermodynamic behavior of our model.

A natural description of the pair amplitude ψ_m is as a planar spin of length Δ_m pointing in a direction that makes an angle ϕ_m with a fixed axis. The thermal (Boltzmann) probability of the length distribution is given primarily by $\mathcal{F}_0(\{\Delta_m\})$ of Eq.(2b) and the term in Eq.(2c) may be thought of as the coupling between such 'spins'. The temperature $T^*(x)$ can be identified roughly as that at which the 'spin' at each bond lattice site acquires a sizable length locally without any global ordering of the angles, whereas the 'antiferromagnetic' ($C > 0$) nearest-

neighbor interaction leads to global order (d-wave superconductivity) setting in at T_c. The two temperatures are well separated for small x because A, B and C are so chosen that $T^*(x \simeq 0) >> T_c$. The region between T^* and T_c is the pseudogap regime where in the spin language, antiferromagnetic short-range correlations grow with decreasing temperature, its length scale diverging at T_c. There is considerable experimental evidence for this view [5–7], though there is also the alternative view that $T^*(x)$ is associated with a new long-range order, e.g. d-density wave (DDW) [37] or time reversal symmetry breaking circulating currents [38].

The BCS theory and conventional GL theory in which the 'spin' formation and ordering temperatures are the same are limiting cases of this scenario. Something like this is expected to happen in cuprates near x_c (Fig.2) as also follows from our functional. The state below T_c has nonzero order parameter $\langle \psi_m \rangle$ for a system above two dimensions, and is a Berezinskii-Kosterlitz-Thouless (BKT) [39–41] bound vortex state with quasi long range order in two dimensions, in which case T_c is identified with the vortex unbinding temperature T_{BKT}. In the former case, the order parameter is the sublattice magnetization $\Delta_d(x, T) = |\langle \psi_m \rangle|$ with a **k**-dependent gap $\Delta_{\mathbf{k}} = (\Delta_d/2)(\cos k_x a - \cos k_y a)$. The interlayer coupling can be described, a la Lawrence and Doniach [42], by adding say a nearest-neighbor coupling between 'spins' on different layers to our functional in Eq.(2). Since this is in practice relatively small (the measured anisotropy ratio in Bi2212 is about 100, for example [43]), it makes very little difference quantitatively to most of our estimates which generally neglect this coupling. For instance T_c calculated by estimating the BKT transition temperature (T_{BKT}) from MC simulation of the two-dimensional model of Eq.(2) (See Section III) is expected to be very close to the actual transition temperature in the anisotropic 3D model with such small interlayer coupling.

A conventional GL theory of cuprate superconductivity would involve a functional similar to that in Eq.(1) (but with additional terms allowed by symmetry) with $\psi(\mathbf{r})$ the d-wave superconducting order parameter, and the coefficient so chosen that a mean-field treatment of the free energy leads to a dome-shaped $T_c(x)$ curve similar to that found in experiments. However, a mean-field treatment and the conclusions obtained from it would not be reliable because of the smallness of the superconducting coherence length in the cuprates and consequent large fluctuation effects. In particular, the pseudogap temperature T^* (which is much larger than T_c for small x, and goes to T_c as x increases) would be absent in such a theory. By contrast, we assume here that the basic low-energy Cooper pair degree of freedom in the cuprates is the bond pair, give a physical meaning to T^* as a pair magnitude crossover temperature, and describe the regime between T^* and T_c as one in which the correlation length associated with superconducting fluctuations of d-wave symmetry grows and diverges at T_c. The effect of these fluctuations is found to be crucial for many physical properties, e.g. the Fermi arc phenomenon, and the filling of the antinodal pseudogap as T rises to T^*. The superconducting order with d-wave symmetry that sets in at T_c is an emergent collective effect, arising from the short-range $\psi_m^* \psi_n$ interaction, much as long-range Neel order arises from an antiferromagentic coupling between nearest-neighbor spins.

GL theories for cuprates have been proposed by a large number of authors, arising either out of a particular model for electronic behavior and often coupled with the assumption of a particular 'glue' for binding electrons into pairs [44–46], or out of lattice symmetry considerations [47, 48]. The functional in Eq.(2) is consistent with square lattice symmetry and, in principle, does not assume any particular electronic approach (weak coupling or strong correlation, for example) or a mechanism for the 'glue'. However, some of the properties of the coefficients are natural in a strong electron correlation framework. For example, mobile holes in such a system can cause a transition between a state in which there is a Cooper pair in the x directed ij bond (Fig.1) to one in which the Cooper pair is in an otherwise identical but y directed bond jk nearest to it (or vice versa), thus leading to a nonzero term $\mathcal{F}_1$ in Eq.(2). This is probably connected with the observed [49] empirical correlation between T_c and the diagonal or next-nearest-neighbor hopping amplitude of electrons in the Cu lattice.

B. Parameters of the Functional

The coefficients A, B and C are chosen to be consistent with experiments. Specifically, the coefficients are as follows:

$$A(x,T) = A_0 \left[T - T_0 \left(1 - \frac{x}{x_c} \right) \right] e^{T/T_p}, \quad (3a)$$

$$B = B_0 T_0, \quad (3b)$$

$$C(x) = x C_0 T_0, \quad (3c)$$

We require Δ_m to have dimensions of energy $[E]$ (or temperature for Boltzmann constant $k_B = 1$) and hence A_0, B_0 and C_0 have dimensions of $[E]^{-2}$, $[E]^{-4}$ and $[E]^{-2}$ respectively. They are rewritten in terms of T_0 as well as three dimensionless parameters f, b and c so that $\mathcal{F}$ carries dimension of energy as well. We thus have, $A_0 = (f/T_0)^2$, $B_0 = b(f/T_0)^4$ and $C_0 = c(f/T_0)^2$. We choose b and c to have values of order unity and fix them for different hole doped cuprates by comparing $\Delta_0(x)$, $T^*(x)$ and T_c^{opt} obtained from the theory with experiments (see below for details).

The two temperature dependent parts of A as given above arise as follows. The part $[T - T_0(1 - x/x_c)]$ reflects our identification of the zero of $A(x, T)$ with the pseudogap temperature and the experimental observation that the pseudogap region extends downwards nearly linearly

from $T = T_0$ at $x = 0$ to $T = 0$ for $x = x_c$. The relation between this straight line $T_l^0(x)$, the experimental $T^*(x)$ and the related quantities $T_{ms}^{0,1}(x)$ (obtained from a maximum slope criterion, Section V) as well as $T^{an}(x)$ (obtained from the antinodal gap filling criterion for the electron spectral function, Section VIII) is shown in Fig.7 and Fig.16. The exponential factor e^{T/T_p} suppresses $\bar{\Delta}(x,T)$ at high temperatures ($T >> T_l^0(x)$) with respect to its temperature independent equipartition value $\sqrt{T/A(x,T)}$ which will result from the classical functional (Eq.(2)) being used well beyond the near proximity of any critical temperature where it is valid. Such a suppression is natural in a degenerate Fermi system; the relevant local electron pair susceptibility is rather small above the pair binding temperature and below the degeneracy temperature. The temperature scale T_p is of order T_0, this being the energy scale for pair binding. We take it to be T_0 unless stated otherwise. In all the calculations below, we choose $x_c = 0.3$ and $b = 0.1$ (except in Fig.4(b)). b along with T_p controls the temperature dependence of $\bar{\Delta}(x,T)$, especially the decrease of $\bar{\Delta}(x,T)$ across the 'pseudogap temperature' line $T^*(x)$ and other details such as the height of the specific heat hump around $T^*(x)$. Values of f, c and T_0 can be fixed for a variety of cuprates by comparing zero temperature gap $\Delta_0(x)$, $T^*(x)$ and T_c^{opt} with experiments. For example, a choice of parameters, roughly suitable for Bi2212, which has an experimental $T_c^{opt} \simeq 91$ K, gives $f \simeq 1.33$, $c \simeq 0.3$ with $\Delta_0(x = 0) \simeq 82$ meV, $T_0 \simeq 400$ K and $T_{BKT}^{opt} \simeq 72$ K ($T_c^{opt} \simeq 110$ K from single site mean field theory, see Section III). Unless otherwise stated, we have used the above choice of parameter values in the rest of the paper.

III. SUPERCONDUCTING TRANSITION TEMPERATURE $T_c(x)$

The superconducting state is characterized by macroscopic phase coherence. For superconductivity in cuprates described by the functional (Eq.(2)) this means a nonzero value for the superfluid stiffness or superfluid density $\rho_s(x,T)$ given by the formula [50],

$$\rho_s = -\frac{C}{2N_b} \langle \sum_{m,\mu} \Delta_m \Delta_{m+\mu} \cos(\phi_m - \phi_{m+\mu}) \rangle$$
$$-\frac{C^2}{2N_b T} \sum_\mu \langle (\sum_m \Delta_m \Delta_{m+\mu} \sin(\phi_m - \phi_{m+\mu}))^2 \rangle$$
$$(4)$$

where the subscript $m + \mu$ refers to $\mathbf{R}_m + l\hat{\mu}$ with $\hat{\mu}$ running over x and y directions in the bond lattice coordinate system (rotated by 45^0 with respect to the x-axis shown in Fig.1), $l = a/\sqrt{2}$ is the spacing of the bond lattice, and N_b is number of sites in the bond lattice ($N_b = 2N$). The superconducting transition temperature $T_c(x)$ is the highest temperature at which $\rho_s(x,T)$ is nonzero. We use

this fact to obtain $T_c(x)$ in single-site and cluster mean-field theories (the relevant details are summarized in Appendix A). As mean field approximations are known [36] to overestimate the transition temperature, we treat the effect of fluctuations in the model of (Eq.(2)) through MC simulations. In these simulations, the standard Metropolis sampling scheme [51] has been used for planar spins $\{\mathbf{S}_m = (\Delta_m \cos \phi_m, \Delta_m \sin \phi_m)\}$, whose lengths are controlled mainly by $\mathcal{F}_0$ (Eq.(2b)). Simulations have been carried out for a 100×100 square lattice (bond lattice) with periodic boundary condition. Typically, 10^5 MC steps per spin have been used for equilibration and measurements were done for next 3×10^5 (6×10^5 in some cases) MC steps per spin. Simulations were done for the doping range $0 - 0.4$ at various temperatures.

In our two-dimensional model, true long-range order is destroyed by thermal fluctuations, but there is nonzero superfluid stiffness due to vortex-antivortex binding (the BKT transition [39–41]) below a temperature T_{BKT}. We calculate the superfluid stiffness in the MC simulation using the formula of Eq.(4) and use it in conjunction with the Nelson-Kosterlitz criterion [52]

$$\frac{\rho_s(T_{BKT})}{T_{BKT}} = \frac{2}{\pi} \qquad (5)$$

based on the BKT theory to obtain the vortex binding temperature $T_{BKT}(x)$, which is identical to $T_c(x)$ in 2D. The above criterion, appropriate for a fixed length XY model or equivalently a low fugacity 2D vortex gas, might not give an accurate estimate of T_{BKT} for the model of Eq.(2) in the extreme overdoped regime close to $x = x_c$ due to large fluctuations in the magnitudes Δ_m [53]. T_{BKT} obtained using Eq.(5) should presumably be quite accurate in the underdoped and optimally doped regions where the magnitudes effectively become 'frozen' since $T^*(x) >> T_c(x)$ resulting in a description of the model (Eq.(2)) in terms of an effective fixed-length XY model (Appendix C) close to the superconducting transition. These results are shown in Fig.3. Results for the temperature dependence of the superfluid stiffness are presented in Section IV.

The calculated T_c curve is approximately of the same parabolic shape as that found experimentally. The causes for the qualitative disagreement at both ends (see Fig.2) are not difficult to understand. For very small x, as well as for x near x_c, our free energy functional needs to be extended by including quantum phase fluctuation effects. For such values of x, zero point fluctuations are important because the phase stiffness is small. Additionally, low-energy mobile electron degrees of freedom need to be considered explicitly for x near x_c. To include quantum phase fluctuation effects, we supplement the GL functional of Eq.(2) with the following term that describes quantum fluctuations of phases (ϕ_m) at a minimal level [54–56]:

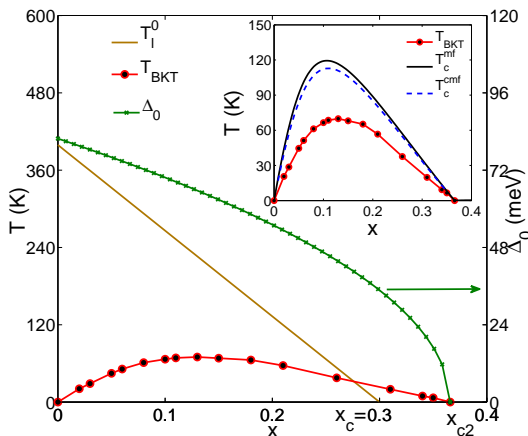$$\mathcal{F}_Q(\{\hat{q}_m\}) = \frac{1}{2} \sum_{mn} \hat{q}_m V_{mn} \hat{q}_n \qquad (6)$$

FIG. 3: Doping dependence of different temperature scales (T_l^0 and T_{BKT}) and the zero temperature gap Δ_0 (Eq.(8b)) are shown in the main plot. Inset: Comparison of the T_c's obtained from single-site mean-field theory and cluster mean-field theory (T_c^{mf} and T_c^{cmf} respectively) (see Appendix A) with the BKT transition temperature T_{BKT} obtained from MC simulation, as discussed in the text.
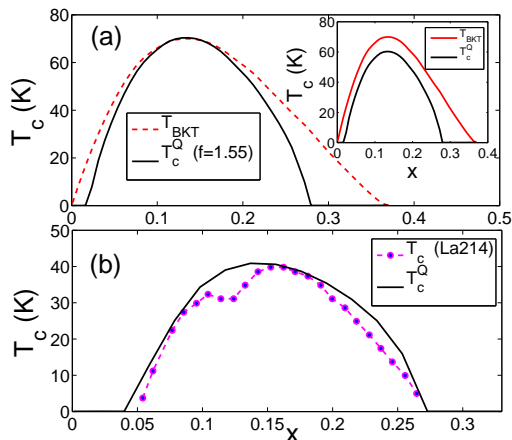

FIG. 4: **(a)** Effect of quantum fluctuation on $T_c(x)$ curve of Fig.3 for $V_0 = 0.09T_0$. The quantum fluctuation renormalizes T_c to T_c^Q throughout the whole x range (Inset). In the main figure, we have taken $f = 1.55$ to change the temperature scale T_0 (= 460 K) while keeping $\Delta_0(x = 0) = 82$ meV (Section II B) so that the optimal value of T_c^Q matches that of T_{BKT} in Fig.3. **(b)** A reasonably good comparison can be obtained with experimental $T_c(x)$ curve for La214 with following choice of parameters (Section II B): $x_c = 0.345$, $c = 0.33$, $b = 0.155$, $f = 1.063$, $T_p = T_0$ and $V_0 = 0.15T_0$ with $\Delta_0(x = 0) = 82$ meV. This choice implies $T_0 = 400$ K. The dip of the experimental T_c around $x \sim 0.12$ is due to the 1/8 'stripe anomaly' [58] which is out of the scope of the present functional of Eq.(2) (see discussion in Section IX).

Here $\hat{q}_m$ is the Cooper pair number operator at site m, and ϕ_m in Eq.(2c) should be treated as a quantum mechanical operator $\hat{\phi}_m$, canonically conjugate to $\hat{q}_m$ so that $[\hat{q}_m, \hat{\phi}_n] = i\delta_{mn}$ [57]. We take the simplest possible form for V_{mn} i.e. $V_{mn} = V_0\delta_{mn}$ for the purpose of demonstrating the effect of quantum fluctuations on the $T_c(x)$ curve (Fig.4), where V_0 is the strength of on-site Cooper pair interaction. We have obtained a single-site mean field estimate of $T_c(x)$, namely $T_c^Q(x)$, including the effect of $\mathcal{F}_Q$ as shown in Fig.4 and discussed in Appendix A. As it is well known, mean field theory overestimates the value of the transition temperature. Hence to compare $T_c^Q(x)$ with $T_{\mathrm{BKT}}(x)$ of Fig.3 as well as with the experimental $T_c(x)$ curve, we scale the T_c^Q calculated using Eq.(A6) by a factor ~ 0.6 in Fig.4. This factor has been estimated by calculating the ratio $T_{\mathrm{BKT}}(x)/T_c^{\mathrm{mf}}(x)$ from Fig.3 (inset). Quantitative agreement for T_c for a specific cuprate, La$_{2-x}$Sr$_x$CuO$_4$ is possible with a particular choice of parameters as shown in Fig.4(b). In this extension of the model, we have ignored the long-range nature of the Coulomb (or charge) interactions, as well as Ohmic dissipation. It has been argued [55] that these two factors together result in a fluctuation spectrum similar to the one obtained in an approximation that ignores both, but retains the short-range part of the charge interaction.

In the remaining parts of the paper, we do not consider quantum phase fluctuations since they modify the results qualitatively only in the extremely underdoped and overdoped regions by aborting the superconducting transition as the phase stiffness $\rho_s(0)$ becomes small (see Fig.5) at these two extremes in our model. In the rest of the x range, these effects are expected to renormalize [59] the values of the parameters of the functional of Eq.(3). We assume that such renormalizations are implicit in our choice of the parameters A, B and C in tune with experimental facts (see Section II B).

IV. SUPERFLUID DENSITY $\rho_s(x, T)$

As mentioned above, we have evaluated the superfluid density ρ_s at finite temperatures using Eq.(4) by MC simulation of our model (Eq.(2)). The results are discussed below along with mean-field results. As we have mentioned in Section III, the transition temperature T_{BKT} can be estimated from the universal Nelson-Kosterlitz jump of Eq.(5), where $\rho_s(T) = 0$ above T_c. We show the results for finite temperature superfluid density in Fig.5(a).

The zero temperature superfluid density can be calculated easily from the ground state energy change due to a phase twist (a 'spin wave') and is given by

$$\rho_s(x, 0) = C\Delta_0^2(x) \qquad (7)$$

where $\Delta_0^2(x)$ is obtained from Eq.(8b) (see Section V). Evidently, $\rho_s(x, 0) \propto x$ for small x (as is implicit in the
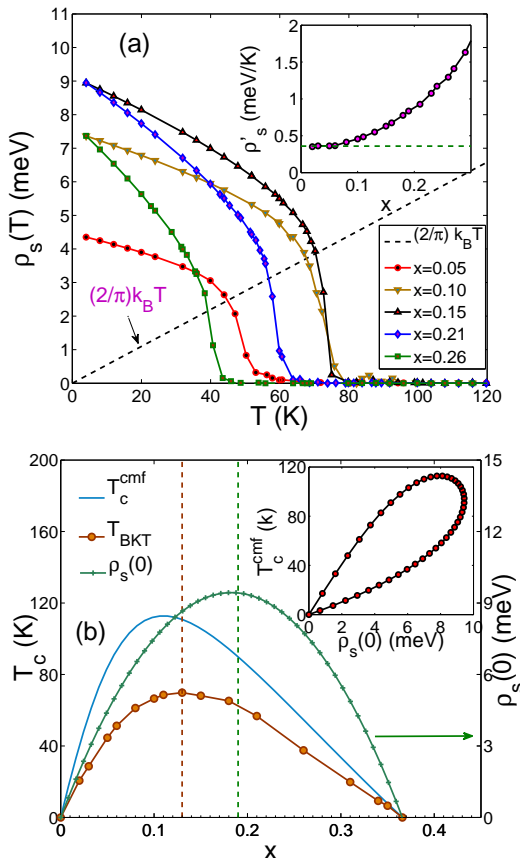
FIG. 5: **(a)** Calculated finite temperature superfluid density for different x values. The dashed line corresponds to the size of universal Nelson-Kosterlitz jump (Eq.(5)) expected at a BKT transition. $T_{BKT}(x)$ has been obtained from the intersection of this line with $\rho_s(x,T)$ vs. T curves. Inset: $\rho_s'(x)$, estimated by fitting $\rho_s(x,T)$ vs. T with a linear form, $\rho_s(x,T) = \rho_s(x,0) - \rho_s'(x)T$. **(b)** Zero temperature superfluid density $\rho_s(x,0)$, as a function of x, compared with $T_{BKT}(x)$ and $T_c^{cmf}(x)$. The superfluid density has been expressed in units of energy (meV) as appropriate in 2D. Vertical dashed lines indicate x's corresponding to optimal values of $\rho_s(x,0)$ and $T_{BKT}(x)$. The inset shows the 'Uemura plot' [16, 17, 19], $T_c(x)$ vs. $\rho_s(x,0)$. The initial part of the upper branch corresponds the underdoped region, where the Uemura relation was inferred [16] originally. The subsequent decrease of $\rho_s(x,0)$ along with T_c in the overdoped regime (lower branch) is observed for example in $Tl_2Ba_2CuO_{6+\delta}$ [17, 19].

choice of C). $T_c(x)$, of course, is also proportional to x for small x, as can be easily verified from Eq.(A5) (see Appendix A), which gives a quite accurate estimate of T_c for low hole doping. Hence, the Uemura relation [16] is seen explicitly to be satisfied for this choice of C. In Fig.5(b) we plot $\rho_s(x,0)$ as a function of x along with $T_c(x)$. $\rho_s(x,0)$ initially increases with x to reach a maximum value (so that $\frac{d\rho_s(0)}{dx} = 0$) slightly on the overdoped side at $x = x_{c_2}/2$ and then ultimately drops to zero at x_{c_2} as T_c also does (see Fig.3), but the optimal $T_c(x)$ and op-

timal $\rho_s(x,0)$ appear, in general, at two different values of doping ($x_{c_2}/2 > x_{opt}$ for the present choice of parameters). A similar behavior is observed in experimental studies of muon-spin depolarization rate, $\sigma_0 \propto \rho_s(x,0)$ of some cuprates which can be sufficiently overdoped [17, 18]. The depolarization rate depends on the local magnetic field at the location of the muon; this has been shown to be proportional to the superfluid stiffness which controls the magnetic response of the superfluid [60]. We also plot $T_c(x)$ as a function of $\rho_s(x,0)$ ('Uemura plot', inset of Fig.5(b))which compares well with experimental plots of T_c vs. σ_0, measured at low temperatures and shown in Refs.17, 19.

At low temperatures the calculated $\rho_s(x,T)$ decreases linearly with T from its zero temperature value i.e. $\rho_s(x,T) = \rho_s(x,0) - \rho_s'(x) T$; the coefficient of the linear term, namely $\rho_s'(x)$ remains more or less independent of x for small x and approaches a constant value as $x \to 0$ on the underdoped side. The same trend can be observed in the experimental data [20, 21] for in-plane magnetic penetration depth λ_{ab}, where $\lambda_{ab}^{-2} \propto \rho_s$. It is interesting that a model for superconductivity such as ours, which does not explicitly include electron degrees of freedom leads to a linear decrease [61, 62], in the light of the fact that the linear dependence has been attributed to thermal, nodal quasiparticles of the d-wave superconductor [1].

V. AVERAGE LOCAL GAP $\bar{\Delta}(x,T)$ AND THE PSEUDOGAP

The energy gap Δ_m is a thermodynamic variable with a certain probability distribution given by the functional of Eq.(2). There is no direct measurement of the energy gap, unlike that of T_c or of the superfluid stiffness discussed in Sections III and IV. The information about the energy gap is obtained via the coupling of the gap (or more precisely, of electron pairs giving rise to the gap) to electrons, photons, neutrons etc. In this section, we compute the thermodynamically averaged local gap $\bar{\Delta}(x,T) = < \Delta_m >$ and compare our results with the broadly observed trends for gaps as inferred from a number of measurements on a variety of cuprates. These trends are for the pseudogap as a function of hole doping x, and for the ratio of the zero temperature gap to the pseudogap temperature $T^*(x)$ as well as to the directly measured superconducting T_c.

Fig.6 shows the dependence of $\bar{\Delta}(x,T)$, calculated in single site mean field theory (see Appendix A), on temperature for different values of the hole doping x. We have checked that the values of $\langle \Delta_m \rangle$ obtained from MC simulations are quite similar to the mean-field results, the main difference being that the singularity of the mean-field values at $T_c(x)$ is smoothed out in the MC results. Note that the quantity $\Delta_m = |\psi_m|$ is *not* the order parameter for superconductivity and its average $\bar{\Delta}(x,T)$ can be (and is) nonzero at temperatures above T_c. The
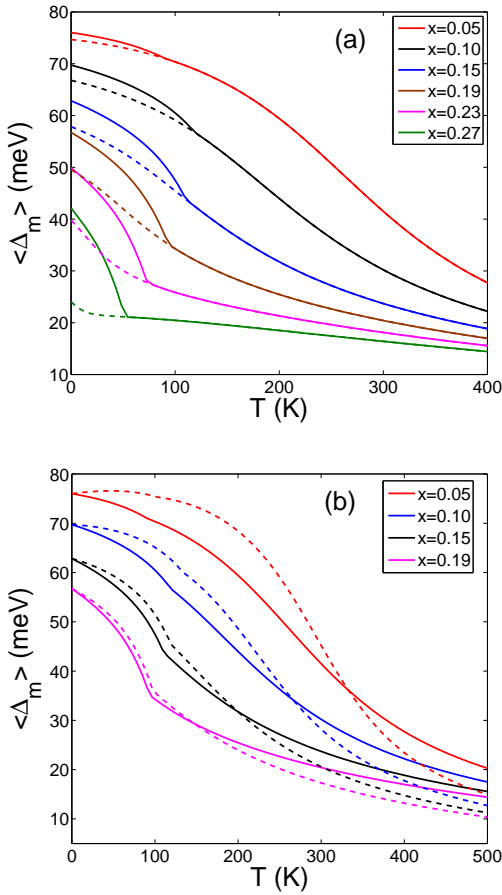
FIG. 6: Panel (a) shows the onset of second gap feature in $\bar{\Delta} = \langle \Delta_m \rangle$ at T_c due to the presence of the C term in Eq.(2). The dashed lines compares $\tilde{\Delta} = \langle \Delta_m \rangle_0$ with $\bar{\Delta}$(see text). Panel (b) compares the temperature dependence of $\bar{\Delta}$ for $T_p = T_0$ (solid lines) and for $T_p = 0.65T_0$ (dashed lines). $\bar{\Delta}$ changes much more rapidly, especially in the underdoped side, with decreasing temperature across $T_{ms}^{0,1}(x)$ for the second case. The results shown here and in Fig.7 were obtained from single-site mean-field theory.
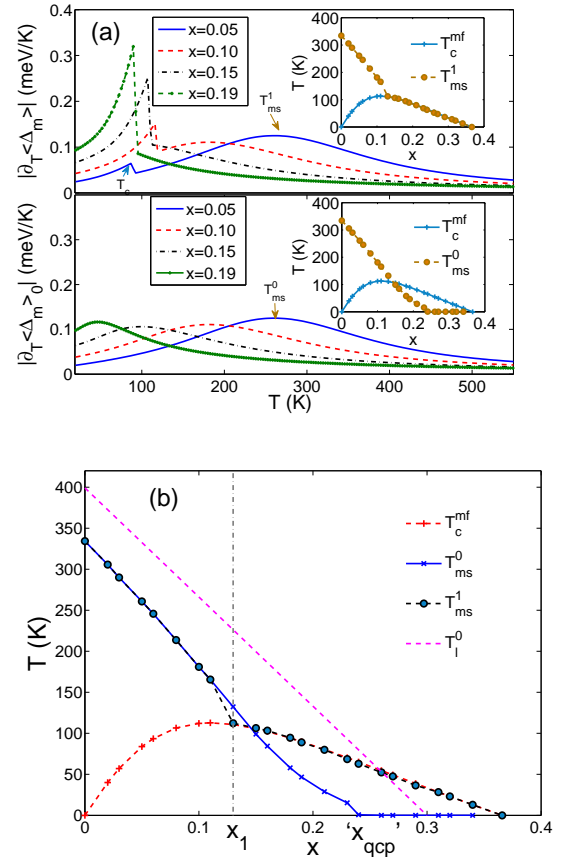
FIG. 7: (a) Extraction of $T_{ms}^1(x)$ from the positions of the maximum of $|\frac{\partial \langle \Delta_m \rangle}{\partial T}| \equiv |\partial_T \langle \Delta_m \rangle|$ vs. T curves (upper panel) at various doping values. Two local maxima appear in the underdoped regime, one sharp peak at T_c and a broad maximum at T_{ms}^1. $T_{ms}^1(x)$ merges with $T_c(x)$ in the overdoped side (inset of upper panel). Similar analysis (lower panel) is carried out on $|\frac{\partial \langle \Delta_m \rangle_0}{\partial T}|$ (see text for definition) to extract T_{ms}^0. (b) Comparison of $T^*(x)$, identified with $T_{ms}^{0,1}$, with other relevant temperature scales; different pseudogap scenarios [7] are naturally embodied in our results, as discussed in the text.

average gap increases smoothly as T decreases; the increase can be rather abrupt or gradual, depending on the parameters (see Fig.6(b)). The part in $\bar{\Delta}(x, T)$ 'turning on' at T_c is generally small. The zero temperature gap $\Delta_0(x) \equiv \bar{\Delta}(x, 0)$, is the sum of these two, a gap which would have been there even in the absence of phase coherence (shown by the dotted line and calculated from $\tilde{\Delta} = \langle \Delta_m \rangle_0$, where the thermal average is evaluated using the single site term $\mathcal{F}_0$ of Eq.(2)) and another, due entirely to phase coherence.

Measurements detect a diminution in the density of electron states, one which depends on the direction of **k** along the Fermi surface. Different measurements (e.g. NMR, resistivity, ARPES etc.) show characteristic changes at temperatures which differs by 20 K to 40 K [5]. The 'pseudogap temperature' $T^*(x)$ is, therefore,

not very well-defined. T^* is generally seen to decrease with hole doping x, nearly linearly, till it 'hits' the $T_c(x)$ curve, around (but slightly beyond) x_{opt}. What happens next is a matter of considerable controversy. Broadly, three scenarios have been argued for, as described for example in Ref.7. One of them [63] suggests that the pseudogap temperature merges with $T_c(x)$ a little beyond optimum doping. Another scenario [8, 37, 38] is that it goes through the $T_c(x)$ dome, reaches zero at a putative quantum critical point x_{qcp}, which controls the universal low temperature behaviour of the cuprate around it in the (x, T) plane. A third [7] is that there is no T^* beyond the hole concentration x_1 at which it 'touches' $T_c(x)$. Operationally, we identify the pseudogap temperature as one at which the absolute value of the slope of $\bar{\Delta}(x, T)$ as a function of temperature is a local maximum,

calling it $T_{\mathrm{ms}}(x)$. In general, this definition leads to two characteristic temperatures. One of them is at T_c because a part of $\bar{\Delta}(x, T)$ suddenly turns on at T_c due to the onset of global phase coherence, leading to a divergence of the temperature derivative at T_c. The other is at a temperature higher than $T_c(x)$ till an x value slightly above x_{opt}. This fact leads to two kinds of behaviour for $T_{\mathrm{ms}}(x)$ (Fig.7) and thus for the pseudogap temperature $T^*(x)$ if these two are identified with each other. If we start from the low doping (small x) side, where $T_{\mathrm{ms}}(x)$ is high and follow it as x increases, noticing its origin in local pairing and existence even when there is no global order, we see that this branch of $T_{\mathrm{ms}}(x)$ denoted as $T_{\mathrm{ms}}^0(x)$ in Fig.7 hits the $T_c(x)$ line at x_1 (Fig.7(b)), goes through the T_c dome to zero temperature at 'x_{qcp}' and continues to be zero thereafter. On the other hand, if beyond x_1 we choose the other solution for $T_{\mathrm{ms}}(x)$ (called $T_{\mathrm{ms}}^1(x)$ in Fig.7), which exists because of the long range order causing 'Josephson' or C term in Eq.(2c), then one has a pseudogap curve which is above $T_c(x)$ till x_1 and is the same as $T_c(x)$ thereafter. These are two of the pseudogap categories mentioned above. Different types of experiments are likely to probe different types of pseudogap. For example, if superconducting phase coherence is destroyed with a magnetic field, so that the C or Josephson term is ineffective, the observed pseudogap behaviour with x is that of the first category.

At zero temperature the phase coherent classical ground state can be represented in terms of nearest-neighbor singlet bond pair fields ψ_m or equivalently $\psi_{i\mu}$ (see Fig.1) as

$$\psi_{ix} = -\psi_{jy} = \Delta_0(x) \quad \forall i, j \tag{8a}$$

$$\Delta_0(x) = \Delta_0(0)\left(1 - \frac{x}{x_{c_2}}\right)^{\frac{1}{2}} \quad x \le x_{c_2},$$
$$= 0 \quad x > x_{c_2}. \tag{8b}$$

Here, $\Delta_0(x)$ is the zero temperature gap (see Fig.3), $\Delta_0(0) = 1/(f\sqrt{b})$ and $x_{c_2} = x_c/(1 - 2cx_c)$ is obtained from $A(x_{c_2}, 0) - 2C(x_{c_2}) = 0$.

Our choice of the values of b and f fixes the ratio $2\Delta_0/T_0 = 2/(f\sqrt{b})$ to be around $3 - 5$, which implies that $2\Delta_0(x)/T^*(x)$ also stays close to these values in the underdoped regime (Fig.8). It has been widely reported [11, 24] that the ratio of the low temperature ('zero temperature') gap to the pseudogap temperature scale, specifically $\Delta_0(x)/T^*(x)$, for a range of hole doping, especially below the optimum x, is about 4.3/2, which is the universal d-wave BCS value [64] for the ratio of zero temperature gap to superconducting transition temperature. Further by choosing $c = 0.3$, the ratio $2\Delta_0(x)/T_c(x)$ near optimal doping is see to be around 10 to 15, as observed in cuprates [9, 11], being substantially higher than the BCS ratio. In Fig.8, the ratio $2\Delta_0(x)/T_c(x)$ is shown to be more or less constant around optimal doping. The increase of this ratio as $(1 - x/x_{c_2})^{-1/2}$ for large x is an artifact of the chosen classical functional.
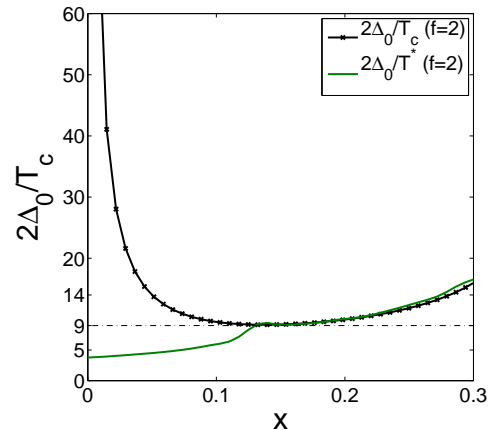

FIG. 8: $2\Delta_0(x)/T_c(x)$ and $2\Delta_0(x)/T^*(x)$ as functions of x. Here $T^*(x)$ refers to $T_{\mathrm{ms}}^1(x)$ (see Fig.7). The long-dashed line corresponds to the nearly constant value of $2\Delta_0(x)/T_c(x)$ near optimal doping.

VI. SPECIFIC HEAT

The electronic specific heat of the superconducting cuprates has been measured in many experiments [26–28]. It consists of a sharp peak near the superconducting transition temperature $T_c(x)$ and a broad hump around the pseudogap $T^*(x)$ [29], both riding on a component that is clearly linear in T at temperatures $T \ge T^*$ in optimally doped and overdoped samples. Here, we summarize theoretical results for the specific heat arising from our functional (Eq.(2)), both with and without magnetic field. A detailed description is given in a separate paper [25]. The functional captures the thermodynamic probability of (bosonic) Cooper pair fluctuations and yields the contribution of these fluctuations to the specific heat. Because of our use of a classical functional, the low temperature behaviour dominated by quantum effects is not properly accounted for; we discuss this below. The low energy electronic degree of freedom ignored in our treatment are the fermionic, non-Cooper-pair ones of the degenerate electron gas. We use the free energy functional (Eq.(2)) to write the specific heat as

$$C_v = \frac{1}{N_b}\frac{\partial \langle \mathcal{F} \rangle}{\partial T} = \frac{1}{N_b}\left[\frac{1}{T^2}\left(\langle \mathcal{F}^2 \rangle - \langle \mathcal{F} \rangle^2\right) \right.$$
$$\left. + \frac{\partial A}{\partial T}\sum_m \left(\langle \Delta_m^2 \rangle - \frac{1}{T}\left(\langle \Delta_m^2 \mathcal{F} \rangle - \langle \Delta_m^2 \rangle \langle \mathcal{F} \rangle\right)\right)\right] \tag{9}$$

where $\frac{\partial A}{\partial T} = (f^2 \exp(T/T_p) + A/T_p)$ for the particular choice of A as in Eq.(3a). Clearly the second term in Eq.(9) arises from the fact that $\mathcal{F}$ is an effective low energy functional whose basic parameters, e.g. A, can be temperature dependent. We evaluate C_v from Eq.(9) for different values of doping x and temperature T by MC
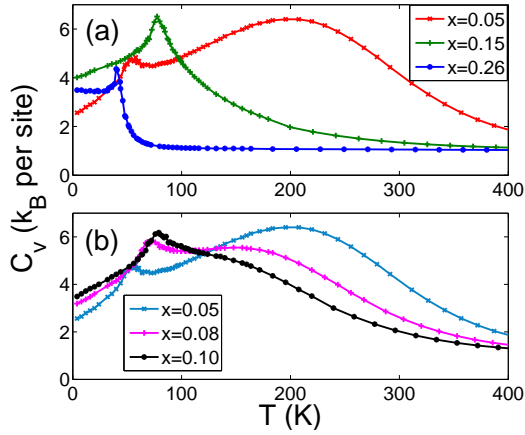
FIG. 9: **(a)** Specific heat obtained from MC simulation of our model (Eq.(2)). Panel **(b)** shows the evolution of the broad maximum around T^* with doping in the underdoped region.

FIG. 10: **(a)** The 'critical' peak appearing near T_c for three values of x. The inset demonstrates the procedure used for the subtraction of the 'non-critical' background (dashed line), as mentioned in the text. **(b)** Analogous plot for the experimental specific heat data for $Y_{0.8}Ca_{0.2}Ba_2Cu_3O_{7-\delta}$ from [27]. Here, x values are estimated using the empirical form of Persland et al. [67]. Again, the inset shows the subtracted background (dashed line) for $x = 0.15$.

sampling of finite 2D systems as mentioned in Section IV. The simulations have been carried out with $f = 2$ (see Section II B) while choosing $\Delta_0(x = 0) \simeq 54$ meV, so that $T_0 = 400$ K.

We notice that in both theory (see Fig.9) and experiment[28, 65, 66], there is a sharp peak in C_v around T_c (or T_{BKT} in our case to be more precise). The peak amplitude increases as x increases, leading to a BCS like shape in the overdoped side. In addition, there is a hump [29], relatively broad in temperature, centered around T^*. The hump is most clearly visible in the calculation for the underdoped regime where T^* and T_c are well separated; its size in the theory depends on A and B (Eq.(3)). In experiments, for the underdoped side, its beginnings can be seen; unfortunately there are very few experiments over a wide enough temperature range to encompass the hump fully in this doping regime. The two features, namely the peak and the hump, and their evolution with x can be rationalized physically. The peak is due the low-energy pairing degrees of freedom which cause long-range phase coherence leading to superconductivity; these are phase fluctuations in the underdoped regime. The hump is mainly associated with the regime where the energy associated with order parameter magnitude fluctuations changes rapidly with temperature. Since this change is a crossover centered around T^* rather than a phase transition, there is only a specific heat hump, not a sharp peak or discontinuity. For small x, $T^* >> T_c$ and so we see that the hump is well-separated from the peak. As x increases, T^* approaches T_c, and in the overdoped regime, these are not separated, and there is no hump, only a peak corresponding to the superconducting transition.

In order to compare our results with experiments, in particular the features related to critical fluctuations near T_c), we remove the contributions that are special to the chosen classical functional and are not connected with the Cooper-pair degrees of freedom in the real systems.
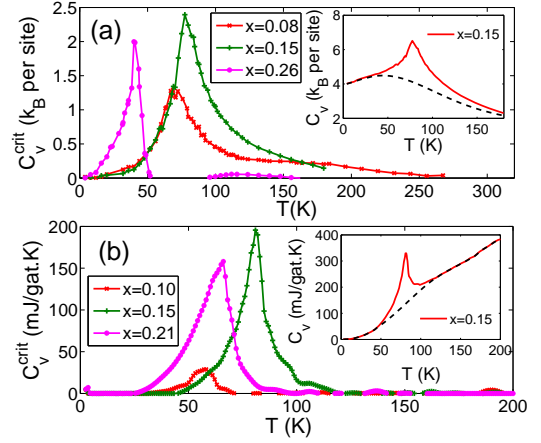
Firstly, at low temperatures, $T << T_c$, the fact that we have a classical functional here leads to a large specific heat of the order of the Dulong-Petit value and there is an additional contribution ($\propto \frac{\partial A}{\partial T}$, see Eq.(9)) due to temperature dependence of A, whereas the actual specific heat is expected to be small because of quantum effects (it is $\sim T^2$ due to nodal quasiparticles [68]). To account for this difference, we compute the leading low-temperature contribution to the specific heat arising from our functional (Eq.(2)). Similarly at high temperatures $T > T^*$, the contribution from pairing degrees of freedom for the actual system is expected to be small, whereas from the functional (Eq.(2)) it is not so due to the simplified from used for the single-site term (Eq.(2b)). We compute C_v from a high temperature expansion for the intersite term in Eq.(2). We interpolate for the specific heat using the low and high temperature expansion results, and subtract the resulting part (includes the hump) from the calculated specific heat. This subtracted specific heat is plotted in Fig.10(a) for three values of doping. These are compared with the experimental electronic specific heat data of Ref. [27] for YBCO after analogous subtraction of a 'non-critical' smooth part obtained from interpolation between low and high temperature regions (excluding the peak) is done (see inset of Fig.10(b)). This procedure also removes linear T contribution to specific heat arising from unpaired low energy electronic degrees of freedom present in the system but not in our functional (Eq.(2)). Since the peaks are large and occur over a narrow temperature near T_c, they are relatively free from possible errors due to the subtraction procedure mentioned above. The experimental and theoretical results
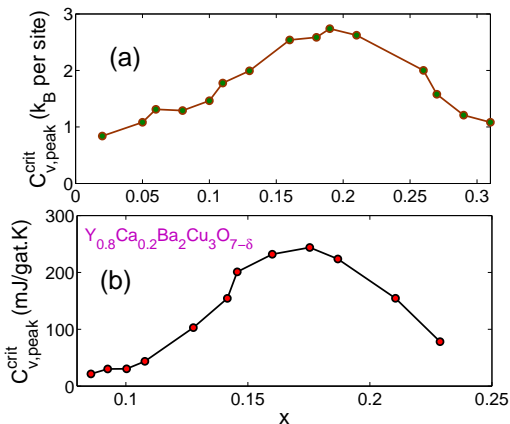
FIG. 11: **(a)** Evolution of the height of the specific heat peak appearing near T_c with doping, compared with the analogous plot **(b)** obtained from experimental data for $Y_{0.8}Ca_{0.2}Ba_2Cu_3O_{7-\delta}$ [27].
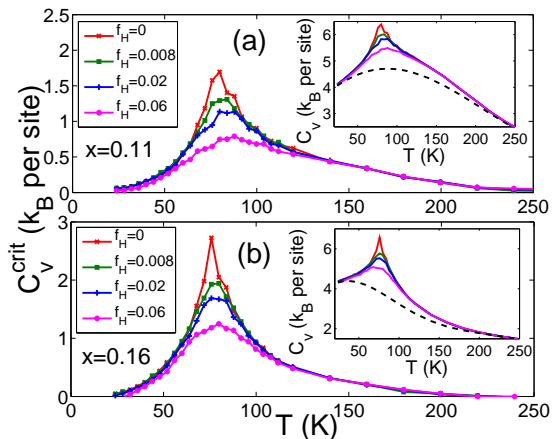

FIG. 12: Effect of a magnetic field on the specific heat peak for **(a)** x=0.11 and **(b)** x=0.16. The subtraction procedure employed in Fig.10 is used here as well, as shown in the insets.

for specific heat peaks are shown separately in Fig.10. We see that they compare well with each other. The qualitative agreement is brought out clearly in Fig.11 where we plot the specific heat peak height with x and compare the dependence with what is observed in experiment. This implies that our model for the bond pairs and their interaction to generate a d-wave superconductor is a faithful representation of the relevant superconductivity related degrees of freedom.

The effects of a magnetic field on the specific heat have been cataloged in [30, 31] where it is found that the specific heat peak near T_c is increasingly smoothed out with magnetic field, but the peak position does not shift by much, especially in highly anisotropic systems such as Bi2212 and Bi2201. This effect is most clearly

visible for small x, and occurs even for magnetic fields as small as a few Tesla. We assume that only the intersite term depends on the vector potential $\mathbf{A}$, via the Peierls phase factor, namely that $(\phi_m - \phi_n)$ in Eq.(2c) is replaced by $(\phi_m - \phi_n - \frac{2e}{\hbar c}\int_{\mathbf{R}_m}^{\mathbf{R}_n}\mathbf{A}.d\mathbf{l})$. The resulting specific heat 'peak' curves obtained from MC simulations are plotted in Fig.12 for two x values at different values of $f_H = Hl^2/\Phi_0$ i.e. the flux going through each elementary plaquette of the bond lattice in units of the fundamental flux quantum $\Phi_0 = hc/(2e)$, where $\mathbf{H}$ is the applied uniform magnetic field perpendicular to the plane (i.e. $\mathbf{H} = H\hat{z}$) and we assume the extreme type-II limit. The results compare well with those of experiment [31].

VII. VORTEX STRUCTURE AND ENERGETICS

We use the functional (Eq.(2)) to find the properties of vortices that are topological defects in the ordered phase. This has been extensively done in the GL theory for conventional superconductors [32]. We use the free energy functional of Eq.(2) at $T = 0$, where it describes the ground state properties, to generate a single vortex configuration by minimizing $\mathcal{F}$ with respect to Δ_m and ϕ_m at each site while keeping the topological constraint of total 2π winding of the phase variables at the boundary of a $N_b \times N_b$ lattice. This is a standard way of generating a stable single $k = 1$ vortex configuration with the vortex core at the middle of the central square plaquette in the computational lattice. The results for $\{\Delta_m, \phi_m\}$ are shown in Fig.13 for two different values of hole doping x, namely $x = 0.10$ (underdoping) and $x = 0.30$ (overdoping). Fig.13(a) shows the order parameter at a point m on the square lattice as an arrow whose length is proportional to the value of Δ_m there, and whose inclination to the x-axis is equal to the phase angle ϕ_m.

We notice that for the underdoped cuprate (e.g. $x = 0.10$) unlike the overdoped one ($x = 0.30$), the order parameter magnitude does not decrease by much as one moves radially inwards from far to the core (Fig.13(b)). This is characteristic of a phase or Josephson vortex whose properties have been investigated for coupled Josephson junction lattice system [69]. We propose therefore that vortices in cuprates in the underdoped regime are essentially Josephson vortices. This is natural here because the Cooper pair amplitude Δ_m has sizable fluctuations only close to T^* which is well separated from T_c ($T_c << T^*$) in the underdoped regime so that near $T = 0$, there are very small Δ fluctuations. Further, for a lattice system (and not for a strict continuum) such a defect is topologically stable since the smallest possible perimeter is the elementary square. On the other hand, beyond optimum doping where, according to Fig.7, T^* coincides with T_c, the order parameter magnitude Δ_m decreases substantially on moving radially inwards towards the vortex core, very much like a 'conventional' superconducting or BCS vortex. The variation of the
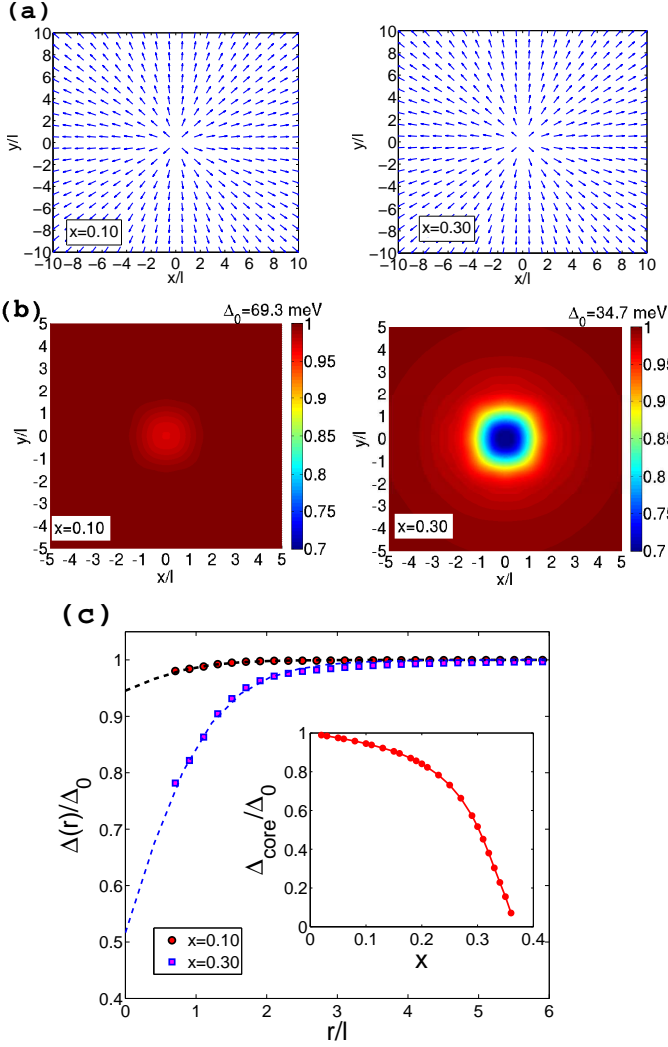
(a)

(b)

(c)

FIG. 14: **(a)** The excess energy of a vortex ΔE_v as a function of system size (see main text) for three values of x. Intercepts of the dashed lines with the vertical axis yield the values of the corresponding core energies E_c. **(b)** E_c is compared with T_c. Like $\rho_s(0)$ (see Fig.5(b)), E_c peaks at $x \simeq 0.19$. The inset shows the proportionality of E_c and T_{BKT} in the underdoped side.

FIG. 13: **(a)** Single vortex configuration for $x = 0.10$ and $x = 0.30$. Arrows indicate the equivalent planar spins. A sublattice transformation has been performed on the phases for convenience of representation. **(b)** Variation of the magnitude of the bond pair field near the vortex core for the aforementioned values of x. The magnitude is plotted in units of its maximum value attained in the bulk, Δ_0 (mentioned at the top of each color bar). **(c)** The angular averaged gap magnitude $\Delta(r)$ (normalized by Δ_0) as function of distance from the core for the two x values. Inset shows the doping dependence of the magnitude at the core, Δ_{core}, estimated by fitting $\Delta(r)$ with $\Delta_0 \tanh(r/\xi_c) + \Delta_{\text{core}}$, while ξ_c and Δ_{core} are kept as fitting parameters.

increasing hole density x.

The core energy E_c of a single vortex is naturally described as the extra energy $\Delta E_v = E_v - E_0$ where E_0 is the energy of the ground state configuration (the Ne′el ordered state in this case) and E_v is the total energy of a single vortex configuration, from which the elastic energy due to phase deformation [36] is subtracted, i.e.

$$\Delta E_v = E_c + \pi \rho_s(0) \ln(R/l) \qquad (10)$$

The quantity R is defined as $R = (N_b - 1)l/\sqrt{\pi}$, where l is the lattice constant of the bond lattice, so that πR^2 is the area of the computational lattice. We plot in Fig.14(b) the core energy E_c as a function of x, both its absolute value and its ratio with T_c. E_c has been estimated from the intercept of the ΔE_v vs. $\ln(R/l)$ (different system sizes) straight line with the energy axis. We notice that for small x, $E_c(x) \propto T_c(x)$ (inset of Fig.14)(b), not surprising from XY model considerations [70].

normalized magnitude of the bond pair field $\Delta(r)/\Delta_0$ with the radial distance r from the vortex core in the two cases is shown in detail in Fig.13(c), which clearly illustrates the difference between the behavior in the two cases. The inset of Fig.13(c) shows the extrapolated values of the magnitudes (Δ_{core}) at the core ($r = 0$) as a function of x, indicating that there is a smooth crossover from a Josephson-like vortex to a BCS-like vortex with
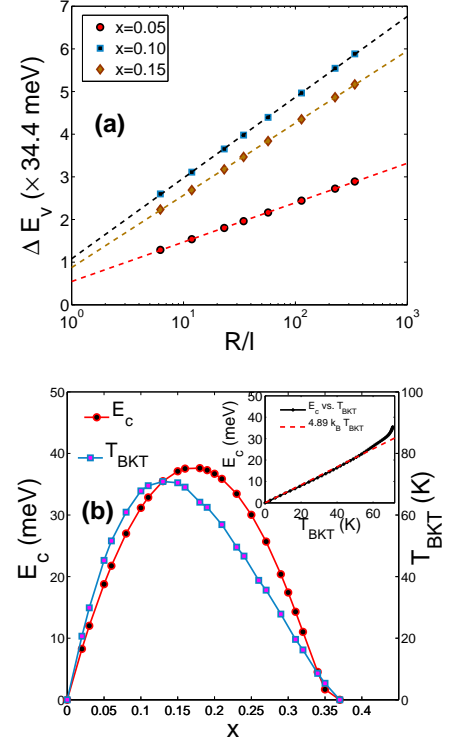
VIII.   ELECTRON SPECTRAL FUNCTION AND ARPES

The cuprate superconductor obviously has both electrons, and Cooper pairs of the *same* electrons, coexisting with each other. In a GL-like approach such as ours, only the latter are explicit, while the former are 'integrated out'. However, effects connected with the pair degrees of freedom are explored experimentally via their coupling to electrons, a very prominent example being photoemission in which the momentum and energy spectrum of electrons ejected from the metal by photons of known energy and momentum is investigated. Since ARPES (angle resolved photoemission spectroscopy) [9, 10] is a major and increasingly high-resolution [71] source of information from which the behaviour of pair degrees of freedom is inferred, we mention here some experimental consequences of a theory of the coupling between electrons and the complex bond pair amplitude ψ_m. The theory as well as a number of its predictions (in agreement with ARPES measurements) are described in detail in Ref.35.

In formulating a theory of the above kind, one faces the difficulty of having to develop a description of electrons in a presumably strongly correlated system such as a cuprate, which is viewed as a doped Mott insulator [1] with strong low-energy antiferromagnetic correlation between electrons at nearest neighbor sites [4]. In particular, one needs to commit oneself to some model for electron dynamics which then implies an approach to the coupling between electronic and pair degrees of freedom. We develop what we believe is a minimal theory, appropriate for low-energy physics. We assume that for low energies $|\omega| \leq \Delta_0$, well-defined electronic (tight-binding lattice) states with renormalized hopping amplitudes t, t', t'' etc. exist and couple to low-energy pair fluctuations $\psi_m = \psi_{i\mu} = \langle (a_{i\downarrow}a_{i+\mu\uparrow} - a_{i\uparrow}a_{i+\mu\downarrow})/2 \rangle$ (see Fig.1). Superconducting order (more precisely, phase stiffness) and fluctuations in it are reflected respectively in the average $\langle \psi_{i\mu}(\tau) \rangle$ and the correlation function $\langle \psi_{i\mu}(\tau)\psi_{j\mu'}^*(\tau') \rangle$ (or its Fourier transform $D_{\mu\mu'}(2\mathbf{q}, iz_m)$, $z_m = 2m\pi/\beta$ being the bosonic Matsubara frequency where m is an integer). A nonzero value of $\langle \psi_{i\mu}(\tau) \rangle$ in the 'AF' long-range ordered phase below T_c leads to the well known Gor'kov d-wave Green's function and quasiparticles with spectral gap $\Delta_{\mathbf{k}} = (\Delta_d/2)(\cos k_x a - \cos k_y a)$. The correlation function $D_{\mu\mu'}(\mathbf{q}, \omega)$ has a generic form for small q and ω which can be related to the functional (Eq.(2)).

The coupling between low excitation energy electrons and low-lying pair fluctuations (both inevitable) leads to a self energy with a significant structure as a function of electron momentum $\mathbf{k}$ and excitation energy ω. Physically, we have electrons (e.g. those with energy near the Fermi energy) moving in a medium of pairs which have finite range 'AF' or d-wave correlation for $T > T_c$ and have long-range order of this kind for $T < T_c$ (in addition to 'spin wave' like fluctuations). The electrons exist both

as constituents of Cooper pairs and as individual entities; the pairs and the electrons are in mutual 'chemical' equilibrium. The energy shift or dynamic polarization of electrons due to this process leads to a number of effects which are described in [35]. For example, for $T > T_c$ we find a pseudogap in electronic density of states which persists till T^*. We get Fermi arcs [9, 10, 72] i.e. regions on the putative Fermi surface where the quasiparticle spectral density has a peak at zero excitation energy in contrast to the pseudogap region where the peak is not at the Fermi energy. The antinodal pseudogap 'fills up' between T_c and T^* with increasing temperature. Below T_c, there is a sharp antinodal quasiparticle peak whose strength is related to the superfluid density as observed in experiment [73]. We also obtain a 'bending' or departure of the $\Delta_{\mathbf{k}}$ vs. $\mathbf{k}$ curve from the mean-field canonical d-wave form due to order parameter or 'spin wave' fluctuations. Here we only outline our theoretical approach and show how a temperature T^{an} can be obtained from the filling in of the antinodal pseudogap above T_c. We find that T^{an} compares well in its magnitude and x-dependence with other measures of the pseudogap temperature scale described in Section V.

The physical quantity of interest is

$$\mathcal{A}(\mathbf{k}, \omega) = -\frac{2}{\pi}\mathrm{Im}[G(\mathbf{k}, i\nu_n \to \omega + i\delta) \qquad (11)$$

(the fermionic Matsubara frequency, $\nu_n = (2n + 1)\pi/\beta$, n being an integer). Assuming translational invariance one has the Dyson equation for G, namely

$$G^{-1}(\mathbf{k}, i\nu_n) = (G^0)^{-1}(\mathbf{k}, i\nu_n) - \Sigma(\mathbf{k}, i\nu_n) \quad (12)$$

where $\Sigma(\mathbf{k}, i\nu_n)$ is the self energy.

$G^0(\mathbf{k}, i\nu_n)$ is described in terms of a spectral density in the usual Lehmann representation [74]. The spectral density for low excitation energies has a Dirac δ-function part i.e. $\mathcal{A}^0(\mathbf{k}, \omega) = z_{\mathbf{k}}\delta(\omega - \xi_{\mathbf{k}})$ where $\xi_{\mathbf{k}}$ is the effective quasiparticle energy measured from the chemical potential μ and $z_{\mathbf{k}}$ (< 1) is the quasiparticle residue. In the 'plain vanilla' or renormalized tight-binding free-particle theory [75, 76] $z_{\mathbf{k}} = 1$ and $\xi_{\mathbf{k}} = \epsilon_{\mathbf{k}}^{\mathrm{eff}} - \mu$ with $\epsilon_{\mathbf{k}}^{\mathrm{eff}} = g_t \sum_{(\mathbf{R}_i - \mathbf{R}_j)} t_{ij} \exp[-i\mathbf{k}.(\mathbf{R}_i - \mathbf{R}_j)]$, so that $G^0(\mathbf{k}, i\nu_n) = 1/(i\nu_n - \xi_{\mathbf{k}})$. The factor g_t is due to correlation effects calculated in the Gutzwiller approximation [76] which projects out states with doubly occupied sites; one further assumes that the renormalized quasiparticles propagate coherently.

We use a standard approximation for $\Sigma(\mathbf{k}, i\nu_n)$ which is shown diagrammatically in Fig.15. This describes a 'phonon' like process neglecting vertex corrections; the propagating electron become a Cooper pair (boson) plus an electron in the intermediate state; these recombine to give a final state electron with the same $(\mathbf{k}, i\nu_n)$. The internal propagator in Fig.15 is the true or full propagator G. However, in common with general practice, we find Σ and thence G by inserting G^0 instead of G in the former. This is known to be quite accurate [74], e.g. for the coupled electron-phonon system.
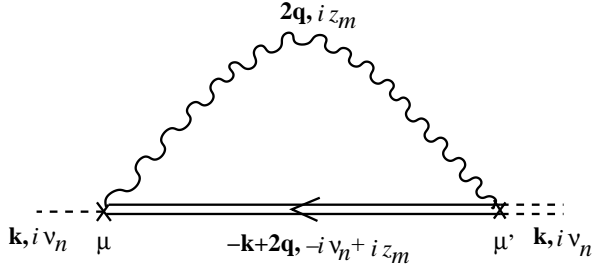
FIG. 15: Self energy approximation used to calculate the electron Green function $G(\mathbf{k}, i\nu_n)$. The wavy line denotes the pair propagator $D_{\mu\mu'}(2\mathbf{q}, iz_m)$ and the line with an arrowhead pointing towards left indicates the full electron Green function $G(-\mathbf{k} + 2\mathbf{q}, -i\nu_n + iz_m)$ (see text). The external lines (dashed) at two ends of the diagram represent bare (left) and true (right) electron propagators. In the static approximation $D_{\mu\mu'}(2\mathbf{q}, iz_m) \equiv (D_{\mu\mu'}(2\mathbf{q})/T^2)\delta_{z_m,0}$ and the summation over the internal bosonic Matsubara frequency in the above diagram drops out (see Appendix B).

In the static approximation valid at high temperatures when the pair lifetime $\tau_p >> 1/(k_B T)$ (see Appendix B), the general algebraic expression for $\Sigma(\mathbf{k}, i\nu_n)$ is

$$\Sigma(\mathbf{k}, i\nu_n) = -\frac{1}{N} \sum_{\mathbf{q},\mu,\mu'} G^0(-\mathbf{k} + 2\mathbf{q}, -i\nu_n) D_{\mu\mu'}(2\mathbf{q}) f_\mu(\mathbf{k}, \mathbf{q}) f_{\mu'}(\mathbf{k}, \mathbf{q})$$

(13)

where N is the total number of Cu sites on a single CuO_2 plane and μ, μ' refer to the direction of the bond i.e. x or y. The static pair propagator is $D_{\mu\mu'}(2\mathbf{q}) = T^2 D_{\mu\mu'}(2\mathbf{q}, 0)$ (see Fig.15) where $D_{\mu\mu'}(2\mathbf{q}) = \sum_{\mathbf{R}} D_{\mu\mu'}(\mathbf{R}) \exp(-i2\mathbf{q}.\mathbf{R})$ with $D_{\mu\mu'}(\mathbf{R}) = \langle \psi_\mu(\mathbf{R}) \psi_{\mu'}^*(\mathbf{0}) \rangle$. Since the XY-like interaction term (Eq.(2c)) between nearest-neighbor bond pairs (see Fig.1) is antiferromagnetic,

$$D_{xx}(\mathbf{R}) = D_{yy}(\mathbf{R}) = -D_{xy}(\mathbf{R}) = D(\mathbf{R}). \qquad (14)$$

Further, the quantity $f_\mu(\mathbf{k}, \mathbf{q})$ is a form factor describing the coupling between an electron and a bond pair. For a tight binding lattice and nearest-neighbor bonds, $f_\mu(\mathbf{k}, \mathbf{q}) = \cos[(k_\mu - q_\mu)a]$.

The pair correlator of Eq.(14) can be written in the standard way [36],

$$D(\mathbf{R}_m - \mathbf{R}_n) = \langle \tilde{\psi}_m \rangle \langle \tilde{\psi}_n^* \rangle \rangle + S(\mathbf{R}_m - \mathbf{R}_n) \qquad (15)$$

where $\tilde{\psi}_m = \Delta_m \exp(i\varphi_m)$ with $\varphi_m = \phi_m$ for x-bonds and $\varphi_m = \phi_m + \pi$ for y-bonds (see Fig.1); $S(\mathbf{R})$ is the fluctuation term. In the long-range ordered state below T_c, the first term is nonzero. In that case, if one neglects effects of fluctuations i.e. $S(\mathbf{R})$ altogether (as is done in mean-field theory), then one obtains the exact Gor'kov self energy form [74] i.e $\Sigma(\mathbf{k}, i\nu_n) = \Delta_{\mathbf{k}}^2/(i\nu_n + \xi_{\mathbf{k}})$ in Eq.(13) and corresponding spectral gap

$\Delta_{\mathbf{k}} = (\Delta_d/2)(\cos k_x a - \cos k_y a)$ in the Néel ordered state. Spin-wave-like fluctuations below T_c can be incorporated through $S(\mathbf{R})$ which generally decays algebraically for large distances i.e. $S(\mathbf{R}) \sim R^{-\eta}$ ($\eta > 0$, its value depends on dimension). Above T_c, $\langle \psi(\mathbf{R}) \rangle = 0$ and the only contribution comes from the fluctuation part. Generically, there is a finite correlation length ξ above T_c and $S(\mathbf{R}) \sim \exp(-R/\xi)$ or $S(\mathbf{q}) \sim 1/[1 + (\xi q)^2]$.

Since we are mainly interested in the spectroscopic features of the pseudogap regime when $T^*(x)$ is perceptibly higher than $T_c(x)$ so that fluctuations in the pair magnitude Δ_m are small and short ranged, we write,

$$\begin{aligned} D(\mathbf{R}) &\simeq \ <\Delta(\mathbf{R})><\Delta(\mathbf{0})> \langle e^{i[\varphi(\mathbf{R})-\varphi(\mathbf{0})]} \rangle \\ &\equiv \bar{\Delta}^2 F(R) \end{aligned} \qquad (16)$$

where $F(R) = \langle e^{i[\varphi(\mathbf{R})-\varphi(\mathbf{0})]} \rangle$ is the phase correlator.

Analytical expression for the self-energy from Eq.(13) can be obtained below T_c, where quasi-long-range order in purely 2D system or true long-range order in anisotropic 3D system occurs, as well as above T_c in the temperature regime where the exponential decay of correlation is governed by a large correlation length ξ [35]. We have carried out calculations [35] for both anisotropic 3D and 2D cases, while incorporating a small interlayer coupling $C_\perp$ (with $C/C_\perp \sim 100$ as suitable for Bi2212) in Eq.(2) for the former. Above T_c the anisotropic 3D system behaves effectively as 2D [77] and our results for various spectral properties are quantitatively similar and even below T_c, for this large anisotropy ratio, qualitative features are the same for both the cases. Hence, we present here the results for the pure 2D system. More specifically, here we have used the form

$$F(R) = \left(\tilde{\Lambda} R \right)^{-\eta} e^{-R/\xi} \qquad (17)$$

to calculate the self energy (Eq.(13)). Here $\tilde{\Lambda}$ is related to the upper wave-vector cutoff of the lattice and $\eta = T/(2\pi\rho_s)$ below T_c where $\xi \to \infty$. Above T_c, we have set $\eta = \eta_{\text{BKT}} = 0.25$. A combination of MC simulation and well-known Kosterlitz-Thouless renormalization group relations has been used to estimate $\xi(x, T)$ from the functional (Eq.(2)) (see Appendix C for details). The self energy $\Sigma(\mathbf{k}, i\nu_n)$ obtained using the form of $F(R)$ in Eq.(17) evolves smoothly from below T_c (superconducting state) to above T_c (pseudogap state).

For $\mathbf{k}$ on the Fermi surface [78] in the antinodal region, we calculate $\mathcal{A}(\mathbf{k} = \mathbf{k}_{\text{an}}, \omega)$. Above T_c but below a certain temperature (denoted as T^{an}), two peaks appear in $\mathcal{A}(\mathbf{k}_{\text{an}}, \omega)$ at nonzero ω, one at $\omega < 0$ and another at $\omega > 0$, signaling the presence of a pseudogap above T_c. The antinodal gap (denoted as Δ_{an}) can be defined from the position of the peak at negative energy ($\omega < 0$). This quantity has been plotted in Fig.16(a) as a function of temperature for a few values of x.

The quantity Δ_{an} goes to zero rather abruptly at T^{an}, though the average local gap $\bar{\Delta}$ is non zero above T^{an} (see Fig.6). The antinodal pseudogap fills in at this temperature [35]. In Fig.16(b), T^{an} is plotted as a function of x.
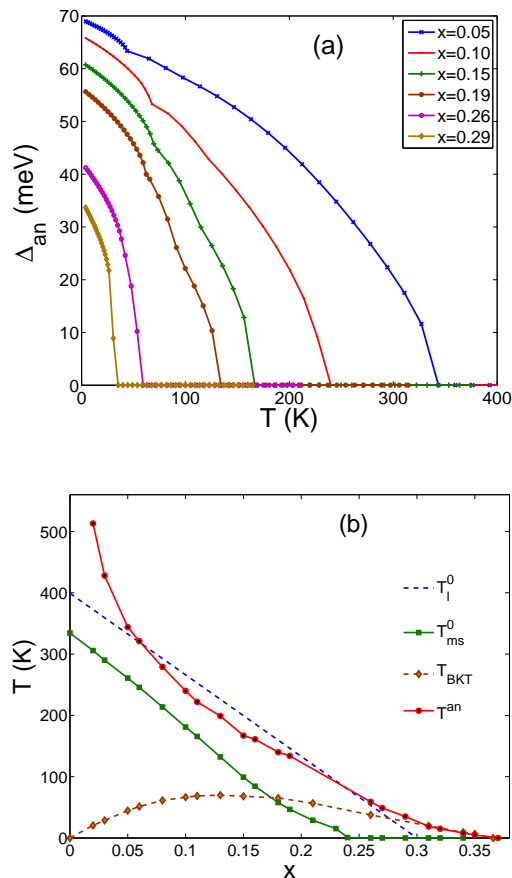
FIG. 16: **(a)** Variation of antinodal gap Δ_{an} with temperature. Slope discontinuities in Δ_{an} vs. T curves correspond to T_c (T_{BKT}). **(b)** Pseudogap temperature scale T^{an} obtained from the antinodal gap filling criterion mentioned in the main text. $T^{\mathrm{an}}(x)$ is compared with other temperature scales, $T_l^0(x)$, $T_{\mathrm{ms}}^0(x)$ and $T_{\mathrm{BKT}}(x)$. Here, we have taken the nearest-neighbor hopping $t = 300$ meV and the next-nearest-neighbor hopping $t' = -t/4$ [81].

We notice that this temperature is close to various pseudogap related temperatures e.g. the somewhat arbitrary linear $T_l^0(x)$ used in Eq.(2), as well as the temperature scale $T_{\mathrm{ms}}^0(x)$ estimated from the temperature dependence of the local gap magnitude. The x-dependence of T^{an} is similar to that of T^* as inferred from ARPES [79] as well from various other probes such as Raman spectroscopy [12] and spin susceptibility [5, 8] over a rather large range of x.

The picture used in our calculation continues to regard the electrons as coherent at all temperatures whereas there is experimental evidence [80] that the incoherence temperature is proportional to x so that it is rather small for small x. Also, for very small x, the holes tend to localize, so that a renormalized band theory implying extended homogeneous electronic states is inappropriate.

IX. DISCUSSION AND FUTURE PROSPECTS

We mention here some obvious directions in which the functional and the approach used here need to be developed. One is to obtain other testable/experimentally measured consequences of the proposed functional. For example in a magnetic field, the intersite term in Eq.(2) has its phase altered by Peierls phase factor, as we have mentioned at the end of Section VI. One should use this to find the $T_c(H)$ curve for different values of doping x and thence the 'bare' coherence length ξ_0 defined through the phenomenological equation, $\frac{1}{T_c}\left(\frac{dT_c}{dH}\right)_{T=T_c} = \left(\frac{\xi_0^2}{\Phi_0}\right)$. The charge related response of a system described by Eq.(2), e.g. the diagonal and off-diagonal components of the conductivity tensor, $\sigma_{xx}(H, T > T_c)$ and $\sigma_{xy}(H, T > T_c)$, and the Nernst coefficient $\alpha_{xy}(H, T > T_c)$, needs to be calculated and compared with experiment. Slightly farther afield, the coupling of the field ψ_m to different probes will enable one to analyze experimental results obtained e.g. from scanning tunneling spectroscopy, Raman spectroscopy and neutron scattering. A generalization to a quantum ψ_m functional and inclusion of other time-dependent effects, e.g. Coulomb interaction and dissipation may enable one to describe quantum phase-fluctuation effects, which are specially prominent (and decisive) for extreme underdoping [82].

A very peculiar feature of cuprates is the unusually large proximity effect [83] observed in them. While XY-spin-like models have been proposed for this [84], a complete understanding of the size, temperature and doping dependence etc. does not exist. It is possible that the present theory can be adapted to address this question.

The theory presented needs to be extended in many major ways. For example, there is a lot of experimental evidence [4] that the system is a Mott insulator at $x = 0$, with a large superexchange $J_{ij} \sim 0.15$ eV., as well as for low-energy magnetic correlations in doped cuprates. This antiferromagnetic interaction evolves into superconductivity for surprisingly small hole doping, $x \geq 0.05$. While the crossover and the possibility of coexistence have been investigated at $T = 0$ [85–87], there is need for a coupled functional for these two bosonic degrees of freedom that goes over to the kind of theory we have described above at large x, while it describes an antiferromagnetic Mott insulator at $x = 0$ and persistent spin correlations (including spin density wave correlations) at $x \neq 0$. Similarly there is considerable evidence for other kinds of correlations, e.g. nematic [88], stripes [89], checkerboard [90], and charge density wave [91] whose significance varies with material, doping (including commensuration effects [58]) and temperature. An appropriate GL like functional is one way of exploring the details of this competition: attempt in this direction already exist [92].

The cuprate properties are very sensitive to certain impurities e.g. Zn replacing Cu. Whether this can be described well in a GL like theory is an interesting question. The effect of impurities or in-plane/intra-plane disorder

is an even more general question in terms of its effect on pairing degrees of freedom as well as incorporation of this effect in a this kind of picture. A subject of basic interest in cuprate superconductivity is the possibility of time-reversal symmetry breaking associable with T^* [38]. There are at least two observations, one of Kerr effect [93] and another of ferromagnetism with lattice symmetry [94], which seem to point to time reversal symmetry breaking below T^*. Since these involve spontaneous long-range order in circulating electric currents, each within a single unit cell of the lattice, and these currents can be modeled in a GL functional, one can explore this novel phase and its consequences in our theory.

In conclusion, we believe that the phenomenological theory proposed and developed here not only ties together a range of cuprate superconductivity phenomena qualitatively and confronts them quantitatively with experiment, but also has the potential to explore meaningfully many other phenomena observed in them.

Appendix A: Mean Field Theory

We describe here various approximate solutions for the properties of the lattice functional (Eq.(2)). The approximations discussed here are single-site mean field theory and cluster mean field theory. We also make use of several well-known results from the Berezinskii-Kosterlitz-Thouless theory [36, 40, 41] for XY spins in two dimensions, in combination with Monte Carlo simulation (see Section III). For positive C in Eq.(2c), there is a low-temperature phase with long range 'AF' order (d-wave superconductivity) or broken symmetry (for $d > 2$). The most common approximation for locating and describing this transition is (single-site) mean field theory, in which we self-consistently calculate the staggered 'magnetic field' $\mathbf{h} = (h_x, h_y)$, acting on the planar spins $\mathbf{S}_m = (\Delta_m \cos\phi_m, \Delta_m \sin\phi_m)$, due to its nearest neighbors, assuming it to be the same at each site (modulo the sign change due to the two sublattice 'AF' order).

In such a mean field theory [36, 95], the self-consistent solution is given by

$$h_\alpha = 4C\langle S_\alpha \rangle_0 \quad (\alpha = x, y) \tag{A1}$$

with

$$\langle S_\alpha \rangle_0 = \left(\frac{h_\alpha}{h}\right) \frac{\int_0^\infty \Delta^2 d\Delta P_0(\Delta) I_1(h\Delta/T)}{\int_0^\infty \Delta d\Delta P_0(\Delta) I_0(h\Delta/T)}, \tag{A2}$$

Here, $P_0(\Delta) = \exp\left(-\beta(A\Delta^2 + (B/2)\Delta^4)\right)$ dictates the local distribution (thermal) of gap magnitude, $h =$

$\sqrt{h_x^2 + h_y^2}$ is the magnitude of the 'staggered' field and I_0, I_1 are modified Bessel functions of first kind. The transition temperature T_c (which is denoted as T_c^{mf} in Fig.3) satisfies the implicit equation

$$2C\langle \Delta^2 \rangle_{P_0}|_{T=T_c} = T_c \tag{A3}$$

where $\langle \Delta^2 \rangle_{P_0} = \int_0^\infty \Delta^3 d\Delta P_0(\Delta) / \int_0^\infty \Delta d\Delta P_0(\Delta)$. Other physical quantities, such as the superfluid stiffness, the superconducting order parameter, the internal energy (and its temperature derivative, the specific heat C_v), can be obtained using the self-consistent solution of Eq.(A1). For instance, in this approximation, the superfluid density ρ_s is given by

$$\rho_s = -\frac{C}{2N_b}\langle \sum_{m,\mu} \Delta_m \Delta_{m+\mu} \cos(\phi_m - \phi_{m+\mu})\rangle_0$$
$$= C \sum_{\alpha=x,y} \langle S_\alpha \rangle_0^2, \tag{A4}$$

In reality, the field acting on a 'spin' fluctuates from site to site. The spatially local fluctuations are systematically included in the well-known cluster theories, the oldest of which is the Bethe-Peierls approximation [95], which consists of a single site coupled to the nearest-neighbors which are described by a mean field. We have used it to calculate an 'improved' T_c (T_c^{cmf}), as shown in the inset of Fig. 3.

For small x, where amplitude fluctuations can be neglected, an estimate of T_c (denoted as $T_{c,0}$) is obtained by replacing $\langle \Delta^2 \rangle_0$ in the above relation (Eq.(A3)) by $\Delta_{m,0}^2$ that minimizes the single-site term $\mathcal{F}_0$, so that $\Delta_{m,0}^2 = -A(x,T)/B$ for $x \le x_c$ and $\Delta_{m,0} = 0$ for $x > x_c$. In this approximation,

$$T_{c,0} = \frac{2xc}{2xc+b}\left(1 - \frac{x}{x_c}\right) \quad x \le x_c$$
$$= 0 \quad x > x_c \tag{A5}$$

Here we have neglected the exponential temperature dependence of A (Eq.(3a)). Consequently x_{opt} can also be estimated by setting $\frac{\partial T_{c,0}}{\partial x} = 0$, which gives $x_{\mathrm{opt}} = \frac{1}{2}\left(\sqrt{(b/c)^2 + (2bx_c/c)} - (b/c)\right)$.

If one includes the term $\mathcal{F}_Q$ (Eq.(6)), the self-consistency condition for T_c in Eq.(A3) gets modified in the following manner [57],

$$\left(4C\langle \Delta^2 \rangle_{P_0} \int_0^\beta d\tau \langle \cos\phi_m(\tau) \cos\phi_m(0)\rangle_{\mathcal{F}_Q}\right)_{T=T_c} = 1 \tag{A6}$$

where the average $\langle ... \rangle_{\mathcal{F}_Q}$ is calculated using the eigenstates of $\mathcal{F}_Q$ and the imaginary time on-site phase-phase correlator in Eq.(A6) is given by [57]

$$\langle \cos\phi_m(\tau) \cos\phi_m(0)\rangle_{\mathcal{F}_Q} = \frac{1}{2}e^{-4\tau V_0(1-\tau/\beta)}. \tag{A7}$$

where V_0 is the on-site Cooper pair interaction strength.

Appendix B: Electron Self Energy in Static Approximation

The self energy depicted in Fig.15 can be written in the following form using $G_0(-\mathbf{k}+2\mathbf{q}, -i\nu_n+iz_m)$ for the internal electron propagator,

$$\Sigma(\mathbf{k}, i\nu_n) = \frac{T^2}{N} \sum_{\mathbf{q},m} \frac{D(2\mathbf{q}, iz_m)\mathcal{P}(\mathbf{k},\mathbf{q})}{i\nu_n - iz_m + \xi_{\mathbf{k}-2\mathbf{q}}}, \quad (B1)$$

where $D(2\mathbf{q}, iz_m) = (1/T)\int_0^\beta d\tau \sum_{\mathbf{R}} D(\mathbf{R}, \tau) e^{-i2\mathbf{q}\cdot\mathbf{R}+iz_m\tau}$ is the Fourier transform of the time-dependent propagator and $\mathcal{P}(\mathbf{k}, \mathbf{q}) = [\cos(k_x a - q_x a) - \cos(k_y a - q_y a)]^2$. If the pairs acquire a finite lifetime τ_p, the pair correlator can be represented in terms of the product of the static propagator (Eq.(14)) and a time-dependent part as $D(\mathbf{R}, t) = D(\mathbf{R})e^{-t/\tau_p}$ so that $D(2\mathbf{q}, iz_m) = (1/T)(e^{i\beta/\tau_p}-1)D(2\mathbf{q})/(iz_m + i/\tau_p)$. This form indicates that pair correlations decay temporally with a lifetime τ_p (one can instead take an oscillatory form i.e. $D(\mathbf{R}, t) \sim \cos(t/\tau_p)$ but this does not change our main conclusion). One can perform the summation over the bosonic Matsubara frequencies (z_m) in Eq.(B1) with the aforementioned form of $D(2\mathbf{q}, iz_m)$ and obtain

$$\Sigma(\mathbf{k}, iz_m)$$
$$= \frac{1}{T} \sum_{\mathbf{q}} \frac{D(2\mathbf{q})\mathcal{P}(\mathbf{k},\mathbf{q})((1-e^{i\beta/\tau_p})f(\xi_{\mathbf{k}-2\mathbf{q}}) + e^{i\beta/\tau_p})}{i(\nu_n + 1/\tau_p) + \xi_{\mathbf{k}-2\mathbf{q}}}.$$
$$(B2)$$

Here $f(\omega) = 1/(e^{\beta\omega}+1)$ is the Fermi function. When $T >> (1/\tau_p)$ (also $\nu_n >> (1/\tau_p)$ since $\nu_n \propto T$) i.e. inverse pair lifetime is much smaller than T, the self energy given above would effectively reduce to the form given in Eq.(13).

Appendix C: Estimation of Correlation Length ξ

We estimate $\eta = T/(2\pi\rho_s)$ (below T_c) and ξ (above T_c) that appear in Eq.(17). As already discussed, we calculated ρ_s below T_c from our functional in Section IV by performing MC simulation. Correlation length ξ can be estimated by fitting obtained $\rho_s(x, T)$ below T_c with the BKT form, $\rho_s(x, T) = \rho_s[T_c^-(x)][1 + b(x)\sqrt{T_c(x) - T}]$ with $\rho_s(T_c^-)/T_c^- = 2/\pi$, and $b(x)$ and $T_c(x)$ as fitting parameters. BKT RG relates [96] $b(x)$ to the temperature-dependence of ξ above T_c through $\xi(x, T) \simeq a_0 \exp\left[b'(x)/\sqrt{T - T_c(x)}\right]$, where $bb' = \pi/2$ and a_0 is a microscopic length scale of the order of the lattice spacing.

[1] P. A. Lee, N. Nagaosa and X. G. Wen, Rev. Mod. Phys. **78**, 17 (2006).
[2] K. H. Bennemann and J. B. Ketterson (Eds.), The Physics of Superconductors (Vol-I and II), Springer (2003).
[3] J. R. Schrieffer and J. S. Brooks (Eds.), Handbook of High -Temperature Superconductivity: Theory and Experiment, Springer (2007).
[4] M. A. Kastner et al., Rev. Mod. Phys. **70**, 897 (1998).
[5] T. Timusk and B. Statt, Rep. Prog. Phys. **62**, 61 (1999).
[6] S. Hüfner et al., Rep. Prog. Phys. **71**, 062501 (2008).
[7] M. R. Norman, D. Pines and C. Kallin, Adv. Phys. **54**, 715 (2005).
[8] J. L. Tallon and J. W. Loram, Physica C **349**, 53 (2001).
[9] A. Damascelli, Z. Hussain and Z.-X. Shen, Rev. Mod. Phys. **75**, 473 (2003).
[10] See the article by J.C. Campuzano, M.R. Norman and M. Randeria in Ref.2.
[11] O. Fischer et al., Rev. Mod. Phys. **79**, 353 (2007).
[12] T.P. Devereaux and R. Hackl, Rev. Mod. Phys. **79**, 175 (2007).
[13] V. L. Ginzburg and L. D. Landau, Zh. Eksperim. i. Teor. Fiz. **20**, 1064 (1950).
[14] J. Bardeen, L. N. Cooper and J. R. Schrieffer, Phys. Rev. **108**, 1175 (1957).
[15] L. P. Gor'kov, Zh. Eksperim. i. Teor. Fiz. **36**, 1918 (1959)

[Soviet Phys.-JETP **9**, 1364 (1959)].
[16] Y. J. Uemura et al., Phys. Rev. Lett. **62**, 2317 (1989).
[17] Y. J. Uemura et al., Nature (London) **364**, 605 (1993).
[18] C. Bernhard et al., Phys. Rev. Lett. **86**, 1614 (2001).
[19] Ch. Niedermayer et al., Phys. Rev. Lett. **71**, 1764 (1993).
[20] B. R. Boyce, J. A. Skinta and T. R. Lemberger, Physica C **341-348**, 561 (2000).
[21] C. Panagopoulos et al., Phys. Rev. B **60**, 14617 (1999).
[22] M. Le Tacon et al., Nature Physics **2**, 537 (2006).
[23] J. W. Alldredge et al., Nature Physics **4**, 319 (2008).
[24] M. Kugler et al., Phys. Rev. Lett. **86**, 4911 (2001).
[25] S. Banerjee, T. V. Ramakrishnan and C. Dasgupta, in preparation.
[26] J. W. Loram et al., Phys. Rev. Lett. **71**, 1740 (1993).
[27] J. W. Loram et al., J. Phys. Chem Solids **59**, 2091 (1998).
[28] J. W. Loram et al., Physica C **341**, 831 (2000).
[29] T. Matsuzaki et al., J. Phys. Soc. Japan **73**, 2232 (2004).
[30] A. Junod, A. Erb and C. Renner, Physics C **317-318**, 333 (1999) and references therein.
[31] H. Wen eta al., Phys. Rev. Lett. **103**, 067002 (2009).
[32] M. Tinkham, Introduction to Superconductivity, McGraw-Hill, Inc. (1996).
[33] S. Banerjee, T. V. Ramakrishnan and C. Dasgupta, in preparation.
[34] D.N. Basov and T. Timusk, Rev. Mod. Phys. **77**, 721 (2005).

[35] S. Banerjee, T. V. Ramakrishnan and C. Dasgupta, in preparation.

[36] P. M. Chaikin and T. C. Lubensky, Principles of condensed matter physics, Cambridge University Press (1998).

[37] S. Chakravarty et al., Phy. Rev. B **63**, 094503 (2001).

[38] C. M. Varma, Phys. Rev. B **73**, 155113 (2006).

[39] V. L. Berezinskii, Sov. Phys.-JETP **32**, 493 (1973).

[40] J. M. Kosterlitz and D. J. Thouless, J. Phys. C **6**, 1181 (1973).

[41] J. M. Kosterlitz, J. Phys. C **7**, 1046 (1974).

[42] W. E. Lawrence and S. Doniach, Proc. 12th Int. Conf. Low Temp. Phys., E. Kanada, ed. (Kyoto 1970, Keigaku Publ. Co. 1971), p-361.

[43] See the article by T. Schneider in reference [2].

[44] G. Baskaran and P. W. Anderson, Phys. Rev. B **37**, R580 (1988).

[45] M. Drzazga et al., Physics Letters A **143**, 267 (1990); M. Drzazga et al., Z. Phys. B-Condensed Matter **74**, 67 (1989).

[46] L. Tewordt, S. Wermbter and Th. Wlkhausen, Phys. Rev. B **40**, 6878 (1989).

[47] D. L. Feder and C. Kallin, Phys. Rev. B **55**, 559 (1997).

[48] A. J. Berlinsky et al., Phys. Rev. Lett. **75**, 2200 (1995).

[49] E. Pavarini et al., Phys. Rev. Lett. **87**, 047003 (2001).

[50] W. Y. Shih, C. Ebner, and D. Stroud, Phys. Rev. B **30**, 134 (1984).

[51] M. E. J. Newman and G. T. Barkema, Monte Carlo Methods in Statistical Physics, Oxford University Press (1999).

[52] D. R. Nelson and J. M. Kosterlitz, Phys. Rev. Lett. **39**, 1201 (1977).

[53] D. Bormann and H. Beck, J. Stat. Phys. **76**, 361 (1994).

[54] S. Doniach, Phys. Rev. B **24**, 5063 (1981).

[55] E. Roddick and D. Stroud, Phys. Rev. Lett. **74**, 1430 (1995).

[56] M. Franz and A. P. Iyengar, Phys. Rev. Lett. **96**, 047007 (2006); I. F. Herbut and M. J. Case, Phys. Rev. B **70**, 094516 (2004).

[57] R. Fazio and H. van der Zant, Phys. Rep. **355**, 235 (2001).

[58] A. R. Moodenbaugh et al., Phys. Rev. B **38**, 4596 (1988); J. M. Tranquada et al., Nature **375**, 561 (1995).

[59] J. V. Jos′e, Phys. Rev. B **29**, 2836 (1984).

[60] J. E. Sonier, J. H. Brewer and R. F. Kiefl, Rev. Mod. Phys. **72**, 769 (2000).

[61] T. Ohta and D. Jasnow, Phys. Rev. B **20**, 139 (1979).

[62] E. W. Carlson et al., Phys. Rev. Lett. **83**, 612 (1999).

[63] N. Nagaosa and P. A. Lee, Phys. Rev. B **45**, 966 (1992).

[64] H. Won and K. Maki, Phys. Rev. B **49**, 1397 (1994).

[65] P. Curty and H. Beck, Phys. Rev. Lett. **91**, 257002 (2003).

[66] C. P. Moca and B. Jankó, Phys. Rev. B **65**, 052503 (2002).

[67] M. Persland et al., Physica C **176**, 95 (1991).

[68] N. Momono et al., Physica C **233**, 395 (1994).

[69] C. J. Lobb, D. W. Abraham and M. Tinkham, Phys. Rev. B **27**, 150 (1983).

[70] L. Benfatto, C. Castellani and T. Giamarchi, Phys. Rev. B **77**, 100506(R) (2008).

[71] J. D. Koralek et al., Phys. Rev. Lett. **96**, 017005 (2006).

[72] M. R. Norman et al., Nature (London) **392**, 157 (1998).

[73] D. L. Feng et al., Science **289**, 277 (2000).

[74] G. D. Mahan, Many-particle Physics, Kluwer Academic/Plenum Publishers (2000).

[75] P. W. Anderson et al., J. Phys. Condens. Matter **16**, R755 (2004).

[76] B. Edegger, V. N. Muthukumar and C. Gros, Adv. Phys. **56**, 927 (2007).

[77] P. Minnhagen and P. Olsson, Phys. Rev. Lett. **67**, 1039 (1991).

[78] The Fermi surface has been defined from the locus of **k** points for which $\xi_{\mathbf{k}} = 0$ in the Brillouin zone. We have done calculations using other criteria of determining Fermi surface e.g. from the locus of the maximum of $\mathcal{A}(\mathbf{k}, \omega = 0)$. For these different criteria as well, the main features of our results remain unaltered with only slight modifications in the details. The chemical potential μ is calculated by setting $\int_{-\infty}^{\infty} d\omega \sum_{\mathbf{k}} f(\omega) \mathcal{A}(\mathbf{k}, \omega) = 1 - x$ ($f(\omega) = 1/(\exp(\beta\omega) + 1)$ is the Fermi function).

[79] J. C. Campuzano et al., Phys. Rev. Lett. **83**, 3709 (1999).

[80] A. Ino et al., Phys. Rev. Lett. **81**, 2124 (1998).

[81] A. Paramekanti, M. Randeria and N. Trivedi, Phys. Rev. B **70**, 054504 (2004).

[82] I. Hetel, T. R. Lemberger and M. Randeria, Nature Phys. **3**, 700 (2007).

[83] Y. Tarutani et al., Appl. Phys. Lett. **58**, 2707 (1991); R. S. Decca et al., Phys. Rev. Lett. **85**, 3708 (2000).

[84] D. Marchand et al., Phys. Rev. Lett. **101**, 097004 (2008).

[85] M. Ogata and H. Fukuyama, Rep. Prog. Phys. **71**, 036501 (2008).

[86] T. Giamarchi and C. Lhuiller, Phys. Rev. B **43**, 12943 (1991).

[87] A. Himeda and M. Ogata, Phys. Rev. B **60**, R9935 (1999).

[88] S. A. Kivelson, E. Fradkin and V. J. Emery, Nature **393**, 550 (1998).

[89] S. A. Kivelson et al., Rev. Mod. Phys. **75**, 1201 (2003).

[90] J. E. Hoffman et al., Science **295**, 4650 (1995).

[91] C. Castellani, C. DiCastro and M. Grilli, Phys. Rev. Lett. **75**, 4650 (1995).

[92] E. Demler, S. Sachdev and Y. Zhang, Phys. Rev. Lett. **87**, 067202 (2001).

[93] J. Xia et al., Phys. Rev. Lett. **100**, 127002 (2008).

[94] B. Leridon et al., Phys. Rev. Lett. **87**, 17011 (2009).

[95] R. K. Pathria, Statistical Mechanics, Butterworth-Heinemann (1996).

[96] V. Ambegaokar et al., Phys. Rev. B **21**, 1806 (1980).